THE
PHYSICAL REVIEW
A journal of experimental and theoretical physics established by E. L. Nichols in 1893

SECOND SERIES, VOL. 68, NOS. 9 AND 10 NOVEMBER 1 AND 15, 1945

Disintegration Schemes of Radioactive Substances VIII. Co^{60}

M. DEUTSCH, L. G. ELLIOTT,* AND A. ROBERTS**
Massachusetts Institute of Technology, Cambridge, Massachusetts
(Received September 15, 1945)

The radiations emitted in the decay of the two isomers of Co^{60} have been studied by means of a magnetic lens spectrometer and coincidence methods. The five-year isomer decays by emission of negatrons of maximum energy 0.308 ± 0.008 Mev, followed by two gamma-rays in cascade, of energies 1.10 ± 0.03 Mev and 1.30 ± 0.03 Mev, respectively. At least 90 percent of the disintegrations of the 10.7-minute isomer proceed by an isomeric transition of energy 0.056 ± 0.003 Mev, presumably to the five-year level. In the remaining disintegrations negatrons of maximum energy 1.25 ± 0.06 Mev are emitted, probably followed by a single gamma-ray of 1.50 Mev. It is shown that the decay of both isomers is consistent with accepted selection rules for beta- and gamma-ray transitions, indicating a high angular momentum quantum number—four or more—for the five-year level and a low one for the 10.7-minute level. It is pointed out that slow neutron capture by Co^{59} should lead predominantly to the five-year level. Co^{60} is a convenient substance for laboratory gamma-ray standards because of its long half-life and practically homogeneous radiation.

INTRODUCTION

THE two species of cobalt produced by slow neutron or deuteron bombardment of cobalt must be assigned to the mass number 60 since Mitchell, Brown, and Fowler[1] have shown stable cobalt to consist of the single species Co^{59}. Livingood and Seaborg[2] found half lives of 10.7 minutes and 5.3 years, respectively, for the two isomers of Co^{60}. They also reported[3] that the five-year isomer emits negatrons with a main group of maximum energy about 0.2 Mev and a weak group extending to about 0.8 Mev. The energy of the gamma-rays as found by lead absorption was given by them as 1.3 Mev. Of the radiations emitted with the 10.7-minute period, they state that they consist mostly of soft internal conversion electrons.

Nelson, Pool, and Kurbatov[4] studied the beta-rays of the 10.7-minute activity in a semi-circular focusing beta-ray spectrometer and reported finding only a continuous spectrum. From an extrapolation of the Fermi plot they found a maximum energy of 1.35 Mev, but the spectrum actually seemed to extend to about 1.6 Mev. The gamma-rays emitted by the short period were found by them to have an energy of 1.7 Mev, while the long period was reported to emit gamma-rays of 1.5 Mev. In a paper[5] read

* Now with the Canadian National Research Council, Montreal.
** Now at Massachusetts Institute of Technology, Radiation Laboratory.
[1] J. J. Mitchell, H. S. Brown, and R. D. Fowler, Phys. Rev. **60**, 359 (1941).
[2] J. J. Livingood and G. T. Seaborg, Phys. Rev. **60**, 913 (1941).
[3] J. J. Livingood and G. T. Seaborg, Phys. Rev. **53**, 847 (1938).
[4] M. E. Nelson, M. L. Pool, and J. D. Kurbatov, Phys. Rev. **62**, 1 (1942).
[5] M. Deutsch and L. G. Elliott, Phys. Rev. **62**, 558 (1942).

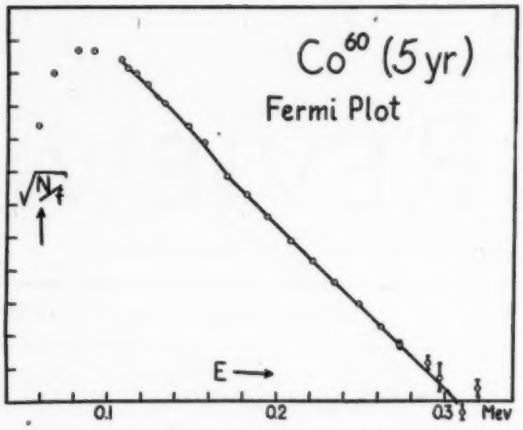

FIG. 1. Fermi plot of the beta-ray spectrum of the 5-year isomer.

to the Physical Society we have reported the results of a study of Co^{60} by means of coincidence and spectrometer techniques described in previous papers of this series.[6] In this paper we shall describe the experiments leading to those results and report some further findings. Although the results, particularly those concerning the 10.7-minute period, are not as complete as those obtained with other activities,[6] we are presenting them at this time because the pressure of other work has prevented the continuation of these studies.

THE FIVE-YEAR ISOMER

Sources of the long-lived species of Co^{60} were prepared by prolonged deuteron bombardment of cobalt metal. The sources usually contained traces of Co^{58} (Paper VII) produced by $(n, 2n)$ and possibly (d, H^3) reactions. The method of chemical purification followed the lines described[6] in paper VI. The specific activity of the material was not high enough for the preparation of a sufficiently strong source which could be considered thin for electrons of such low energy. The shape of the beta-ray spectrum is therefore distorted at low energies by scattering in the source and near the endpoint by the low resolution of the spectrometer which is necessary because of the low intensity available. Figure 1 shows a Fermi plot of the spectrum observed in the short lens spectrometer. A very weak high energy "tail" extending to about 1 Mev was shown to be due to secondary electrons ejected from the source by gamma-rays since its intensity was increased when the source was covered by a thin copper foil. These electrons were subtracted before plotting Fig. 1. The maximum energy of the spectrum as obtained from Fig. 1 is 0.308 $\pm$0.008 Mev.

Figure 2 shows a spectrum of the secondary electrons ejected by the gamma-rays of Co^{60} from a thin lead radiator and from the copper capsule containing the source. The two photoelectron peaks are clearly due to the K electrons of lead ejected by gamma-rays of 1.10 Mev and 1.30 Mev quantum energy, respectively.

The similarity of the spectrum shown in Fig. 2 with that produced by the gamma-rays of Fe^{59} (Paper IV) is rather striking. However, coincidence studies showed the disintegration schemes to be quite different. The number of beta-gamma coincidences per recorded beta-ray of Co^{60} was found to be $3.12\pm0.09\times10^{-3}$ and independent of beta-ray energy. This number is just twice the value observed with a source of Fe^{59} placed in the same standard coincidence arrangement (Paper V). Gamma-gamma coincidences were also observed in the case of Co^{60}, and their number was $1.60\pm0.08\times10^{-3}$ per recorded gamma-ray. Thus there can be no doubt that the two gamma-rays are emitted in successive rather than in alternate transitions. The ratio 2:1 of the fractional beta-gamma and gamma-

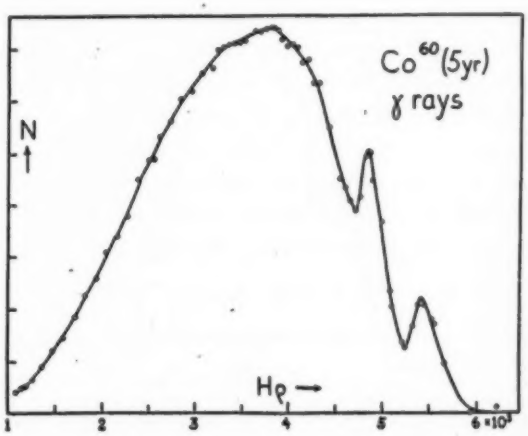

FIG. 2. Secondary electrons ejected by the gamma-rays of the 5-year isomer.

[6] Reference to the earlier papers will be found in paper VI: L. G. Elliott and M. Deutsch, Phys. Rev. 64, 321 (1943), reference 1. The short lens spectrometer has been described by M. Deutsch, L. G. Elliott, and R. D. Evans, Rev. Sci. Inst. 15, 178 (1944).

gamma coincidence rates is, of course, just what one would expect in this case. Sources of Co^{60} are quite convenient gamma-ray standards because of the almost monochromatic radiation and the long lifetime. Co^{60} also provides one of the calibration points of the gamma-ray counter efficiency curve (Paper V). Figure 3 shows the disintegration scheme of Co^{60}. The order of emission of the two gamma-rays is not determined by our experiment.

THE 10.7-MINUTE ISOMER

The half-life of the short-lived isomer is somewhat too short for a thorough study by our usual methods. However, a certain amount of information was gained about its mode of decay.

Since the short half-life does not permit careful chemical purification, we prepared most sources by a slow neutron capture process, using a Szilard-Chalmers process. Sources prepared by deuteron bombardment of cobalt behaved in every way like those prepared by neutron capture, but occasionally radioactive impurities were introduced from the cyclotron chamber.

About 40 grams of potassium cobalticyanide were prepared and dissolved in 500 cc of water. Before exposure about 2 mg of $CoCl_2$ were added as carrier. After exposure the radioactive atoms were collected with the carrier by precipitation with NaOH and H_2O_2. The cobalticyanide had to be purified frequently by precipitation with alcohol, because the peroxide used in the separation seemed to cause formation of interfering compounds.

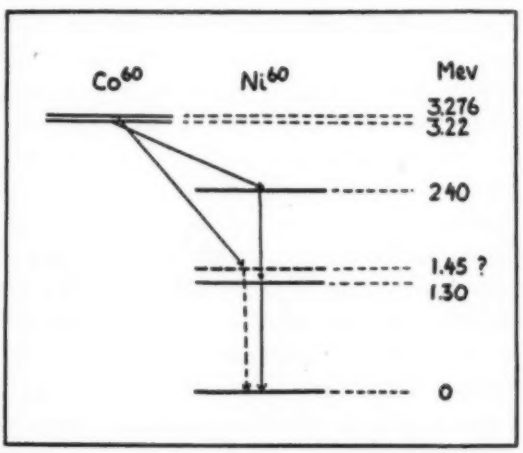

FIG. 3. Probable decay scheme of Co^{60}. The excitation of the level indicated by the dotted line is probably 1.50 Mev. The isomeric transition not clearly indicated in the figure constitutes 90 percent of the disintegrations.

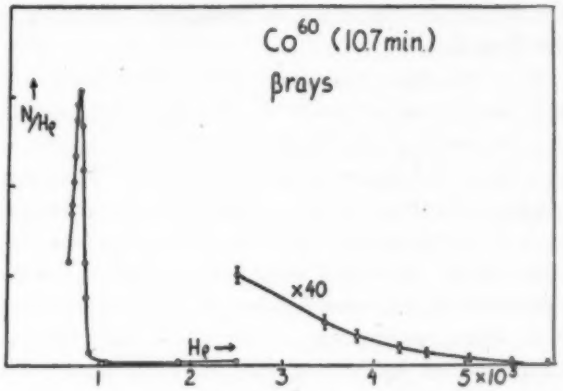

FIG. 4. Beta-ray spectrum of the 10.7-minute isomer. No correction for absorption in the counter window has been applied.

An absorption curve of the beta-rays emitted by the 10.7-minute isomer showed a very soft component of great abundance and another component of maximum range 470 mg/cm². This value corresponds to a maximum energy of 1.15 Mev. Unfortunately the half life of 10.7 minutes is too short to permit careful preparation of sources for spectrometer observations. Sources were prepared by cutting a piece of the filter paper holding the oxide precipitate. Figure 4 shows that, although these sources were rather thick, they allowed us to identify the two components of the beta-radiation. The soft component is seen as a peak of conversion electrons. Its relative intensity is greatly reduced by absorption in the counter window and in the source. The peak occurs at an energy of 48.5 ± 2 Kev. The K and L peaks are not resolved because of the thickness of the source. If the conversion occurs mostly in the K shell, as seems likely from theoretical considerations, the energy of the converted gamma-ray is 0.056 ± 0.003 Mev. If L conversion should be abundant, the gamma-ray energy may be slightly lower. The hard component of the beta-rays is a continuous spectrum. The maximum energy, as found from the rather inaccurate data of Fig. 4, appears to be 1.28 ± 0.06 Mev. This is in fair agreement with the absorption data.[7] We estimate that there are at least ten times as many conversion electrons as

[7] In the preliminary report (reference 5), this value was erroneously given as 1.5 Mev.

disintegration electrons. K x-rays of cobalt were also found.

Since gamma-rays of about 1.7 Mev had been reported to accompany the decay of the 10.7-minute isomer,[4] we studied coincidences between beta-rays and these hard gamma-rays. The conversion electrons were found to be unaccompanied by gamma-rays. The beta-rays, on the other hand, showed $1.3\pm0.4\times10^{-3}$ beta-gamma coincidences per recorded beta-ray, in agreement with the assumption that each beta-ray is accompanied by one gamma-ray of about 1.5 Mev.

The isomeric transition of 0.056 Mev probably leads to the five-year level since no other periods have been observed. The beta-decay, with maximum energy 1.25 ± 0.06 Mev, leads to an excited state of Ni^{60} with an excitation energy of 1.50 ± 0.1 Mev as calculated from the energy balance in the scheme shown in Fig. 3. It seems rather unlikely that this excitation energy could really be 1.30 Mev, involving the same state as the decay of the five-year isomer, but the possibility cannot be entirely excluded without an actual spectrometer measurement of the gamma-ray energy for which sufficient source strength was not available.

DISCUSSION

The disintegration scheme of the five-year level (probably the ground state) of Co^{60} seems quite well established except for the order of emission of the two gamma-rays. The main features of the decay of the 10.7-minute level are also probably correctly given by the scheme shown in Fig. 3.

It seems interesting to investigate whether the decay of both levels can be adequately described by known selection rules for electromagnetic and beta-ray transitions. The ground state of Ni^{60} probably has an angular momentum zero. If we assume that the transition probability for electric dipole and quadrupole radiations is of the same order of magnitude, then the state with 2.4 Mev excitation must have an angular momentum quantum number of at least three, while the intermediate state, with 1.1 Mev or 1.3 Mev excitation, must have angular momentum one or more, with appropriate parity assignments for all states. If the 2.4 Mev level had angular momentum zero, also possible according to selection rules for gamma-ray emission, beta-transitions to the ground state should certainly occur with observable abundance. The five-year beta-decay is probably "first forbidden," involving parity change, and must occur with an angular momentum change of at least one in order to forbid transitions to the intermediate excited state. Thus the five-year level of Co^{60} must have an angular momentum quantum number of at least four. If the beta-decay is of the allowed type, this could be reduced to three. On the other hand, the beta-decay of the 10.7-minute level may be an allowed transition. This is true if the ratio of 1:10 for the ratio of beta-decay to isomeric transition is correct, since the beta-decay rate corresponds then to a half-life (in the absence of the competing transition) of 107 minutes. Since, furthermore, the de-excitation of the resulting state of Ni^{60} seems to proceed by the emission of a single quantum, the angular momentum of the 10.7-minute level of Co^{60} may be low, even zero.

Now let us consider the electromagnetic "isomeric transition." The observed decay constant for this transition is about $\lambda=10^{-3}$ sec.$^{-1}$. Using for the gamma-decay constant the formula given by Segrè[8] (quoted by Helmholtz) and for the conversion coefficients the values given by Hebb and Nelson,[9] we find for electric 2^3-pole radiation $\lambda_3^{(\gamma)}=4\times10^{-2}$ sec.$^{-1}$. The internal conversion coefficient is about 100, giving a total $\lambda_3=4$ sec.$^{-1}$, with K conversion preponderant by a factor of 5. 2^3-pole radiation requires parity change and an angular momentum change of 2 or 3 units. For 2^4-pole radiation we find similarly $\lambda_4^{(\gamma)}=2\times10^{-9}$ sec.$^{-1}$, with the internal conversion coefficient 1000, giving a total $\lambda_4=2\times10^{-6}$ sec.$^{-1}$. Again K conversion would be greater than L conversion by a factor of 3. Electric 2^4-pole radiation involves no parity change and an angular momentum change of 3 or 4 units. The relativistic formula of Dancoff and Morrison (their Eq. (18)) gives values of the conversion coefficients larger by a factor of 3 for 2^3-pole and by a factor of 8 for 2^4-pole radiation. This gives

[8] A. C. Helmholtz, Phys. Rev. 60, 415 (1941).
[9] M. H. Hebb and E. Nelson, Phys. Rev. 58, 486 (1940); also S. M. Dancoff and P. Morrison, Phys. Rev. 55, 121 (1939).

predicted decay constant $\lambda_3 = 12$ sec.$^{-1}$ and $\lambda_4 = 1.6 \times 10^{-5}$ sec.$^{-1}$, as compared with the observed value $\lambda = 10^{-3}$ sec.$^{-1}$. One may conclude that if the theory means anything at all, the angular momentum difference between the two states of Co^{60} should be between two and four, and that there is evidence that it is three or four. This is quite consistent with the evidence from the independent beta-decay of the two states, as discussed above, where it was also shown that the five-year level is probably the one with higher angular momentum.

This apparent agreement with accepted selection rules leads us to consider the neutron capture process by Co^{59}, whose normal state is known[10] to have a nuclear angular momentum quantum number 7/2. This means that upon capture of a slow neutron the excited compound nucleus Co^{60} must be in a state with angular momentum 3 or 4, depending on the relative orientation of the neutron spin. It would, therefore, seem likely that the five-year level should be populated more heavily by the ensuing gamma-ray emission. If the number of steps in which this emission takes place is small, then the known selection rules favor a small angular momentum change. If a large number of gamma-rays is emitted in cascade, then the final result of random changes in angular momentum should still tend to be small, favoring transitions to the five-year level which seems to have angular momentum near four. This effect should be enhanced by the greater statistical weight of states of larger angular momentum. Unfortunately, the available data are very unreliable, because it is not known what fraction of the radiations of the two isomers were detected by the various observers. Horvath and Salant[11] report a total neutron capture cross section 600 times as great as the production of the 10.7-minute isomer, while Sinma and Yamasaki[12] find a ratio 40:1. Granting the great uncertainty of the neutron capture experiments, the results seem to support our assumptions concerning the angular momenta of the two states.

From the disintegration scheme shown in Fig. 3, one can calculate the mass difference between neutral atoms $Co^{60} - Ni^{60} = 2.92 \times 10^{-3}$ a.m.u.

It is a pleasure to acknowledge the friendly cooperation of Professor M. S. Livingston and the cyclotron crew and of Professor J. W. Irvine, Jr. who helped with the chemical procedures. We also wish to thank Professor R. D. Evans for his continued interest.

[10] K. R. More, Phys. Rev. **46**, 470 (1934).

[11] W. J. Horvath and E. O. Salant, Phys. Rev. **59**, 154 (1941).

[12] K. Sinma and F. Yamasaki, Phys. Rev. **59**, 502 (1941).

Shock Wave Pressures in Water Produced by Impact of Small Spheres*

J. HOWARD MCMILLEN**
Department of Biology, Princeton University, Princeton, New Jersey
(Received September 19, 1945)

Microsecond spark shadowgrams were made showing shock waves in water. The waves were produced by spheres $\frac{1}{8}''$ to $\frac{1}{4}''$ in diameter when they struck a water surface with velocities between 2000 and 4800 ft./sec. Pressures in the wave were calculated from measurements of the absence-of-light band. The pressure was found to be greatest at a point directly ahead of the sphere and to fall off to normal pressures near the surface. The waves of large pressures were observed to travel faster than a sound wave and to have velocities in accordance with the measured pressure. Because of the varying strength over the wave front, the waves have the shape of a semi-ellipse. When the entrance velocity V and projection area of the sphere were varied it was found that the pressure varied as $V^{2.17}$. It also increased linearly with the projection area of the sphere. The pressures were shown to be in fair agreement with those calculated from the compression of the water at the sphere's entrance; in the calculation an arbitrary loss of water in the splash was assumed.

WHEN an object moving with high velocity strikes the surface of water, a disturbance is produced which spreads through the water along radial lines with the point of impact as origin. The disturbance consists of a region of increased pressure and density together with a small forward motion of the medium. If the energy in the disturbance is small, the disturbance is propagated as a sound wave, but if it is large, the disturbance travels as a surface of discontinuity and is called a shock wave. While a large number of investigations[1–3] have been carried out on the propagation of shock waves in air, there has been very little reported concerning their formation and transmission through water, especially when the waves have been produced by impact. It was an interest in the relationship between the strength of the shock wave and their method of production which prompted this investigation. The experiment was directed toward determining how the pressure in the wave depended on the shape and kinematical characteristics of the impacting object.

Small spheres were used as the impacting objects because of their radial symmetry. These were shot into the water with high velocities so as to produce waves of strength sufficient to give the shock wave characteristics. The velocity range extended from about 2000 ft./sec. up to the velocity of sound in water 4800 ft./sec. Since the sphere travels with a subsonic velocity and since it is considerably retarded, the wave detaches itself from the sphere soon after it is produced. Thus this investigation has been one of detached waves.

The spark shadowgraph method was used to study these waves. It has been widely used to study shock waves in air[4, 5] ever since its development by Boys[6] in 1893. The method has the advantage of showing the general disposition of the wave at one observation. It is also well suited for measuring the pressure at the front of the wave where the pressure rises abruptly.

APPARATUS AND METHOD

The spark shadowgraphs were produced by light from a point-source spark of short duration. The light traversed a small tank with Plexiglas walls a few microseconds after the missile had struck the surface; the shadow of the shock wave was recorded on a photographic plate

* This work has been carried out under a contract recommended by the Committee on Medical Research between the Office of Scientific Research and Development and Princeton University.
** On leave of absence from Kansas State College, Manhattan, Kansas.
[1] G. I. Taylor and J. W. Maccoll, W. F. Durand's *Aerodynamic Theory* (Verlagsbuchhandlung Julius Springer, Berlin, 1935), Vol. III
[2] A. Busemann, *Handbuch der Experimental Physik*, Vol. 4.
[3] J. Ackeret, *Handbuch der Physik* (Verlagsbuchhandlung Julius Springer, Berlin, 1927), Vol. 7.
[4] D. C. Miller, *Sound Waves Their Shape and Speed* (The Macmillan Company, New York, 1937).
[5] C. Cranz and K. Becker, *Lehrbuch der Ballistik* (Verlagsbuchhandlung Julius Springer, Berlin, 1926), Vol. III.
[6] V. Boys, Nature **47**, 415 (1893).

which was placed just beyond the tank. The experimental arrangement is shown in Fig. 1(a), with the spark S, the tank T, the photograph plate PP, and the missile path G.

The spark was mounted in a brass tube two inches in diameter with a window having an area of 0.006 cm². The electrodes were cut from magnesium rod. A detailed drawing of the spark is shown in Fig. 1(b). The potential across the spark was 4400 volts. The flash discharged four oil-impregnated filter condensers which were connected in parallel giving a capacitance of 0.20 microfarad. Since a discharge of long duration blurs the shock-wave image, the spark was constructed with low resistance leads. Condensers with low resistance supports and plates were also chosen. The arrangement of several condensers in parallel was found to be best as this reduced the total condenser-plate resistance. Since a low capacitance produces a short discharge, the capacitance was kept as low as possible but still sufficiently high to form the desired image on the photographic plate. The duration of the spark was tested by making spark shadowgraphs of spheres traveling in air with a velocity of about 5000 ft./sec.; at this velocity the sphere travels 1.5 mm per microsecond. From the photographs it was estimated that the effective spark-duration did not exceed a tenth of a microsecond.

A wire grid, labeled Q in the figure, triggered the spark when the missile broke one of its wires. The grid was made of No. 32 copper wire spaced about 2 mm apart. Breaking the wire grid operated a thyratron-controlled spark coil which produced a discharge between the trigger electrode and the body electrode in the main spark.

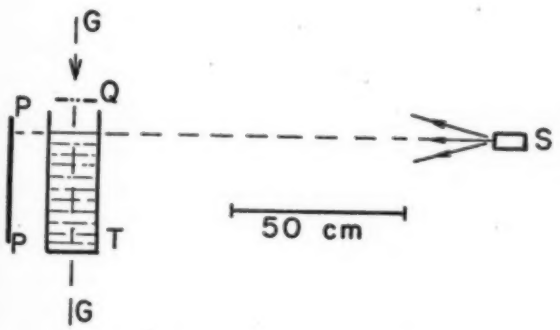

FIG. 1(a). Diagram of apparatus.

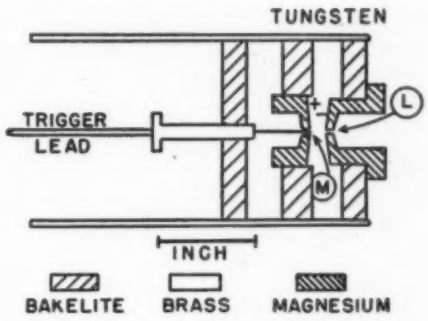

FIG. 1(b). Detail diagram of spark. Light emerges from hole L (drilled with No. 65 drill) after spark is triggered by third electrode in hole M (No. 43 drill).

An adjustable capacitance delay was also incorporated in the circuit.

The tank had two supporting walls of $1\frac{5}{8}$" wood and two transparent walls of $\frac{1}{4}$" Plexiglas. The distance between the wood walls was $14\frac{1}{2}$" and between the Plexiglas $5\frac{1}{2}$"; the water was $10\frac{1}{2}$" deep.

The spark shadowgraph was recorded on a 11×14-inch photographic plate which was placed 17.2 cm from the path of the missile. The path of the missile was also in the center of the tank. Eastman Kodak lantern slide plates of medium contrast were used. They were developed in *D*-72 (one:one) for five minutes.

The spark, 120 cm from the path of the missile, was placed on a line parallel to the water surface and perpendicular to the face of the tank and photographic plate. In order to convert measurements that were made on the plate to corresponding distances at the missile path, a spark shadowgraph picture was made of transparent rulers held in the path of the missile. The shadowgraph was found to have a magnification of 1.11 diameters.

Light rays which deviate from a point along the path of the missile have their deviation angle altered as the rays pass from the water to the air. For small angles near normal incidence, the distance separating two rays incident on the photographic plate was calculated to be 18.2 percent larger than it would have been if no refraction took place. This latter correction was applied to the measurements of the shock wave band widths.

Small steel balls having diameters from $\frac{9}{32}$ to $\frac{8}{32}$ inches were used as missiles. Their diameter

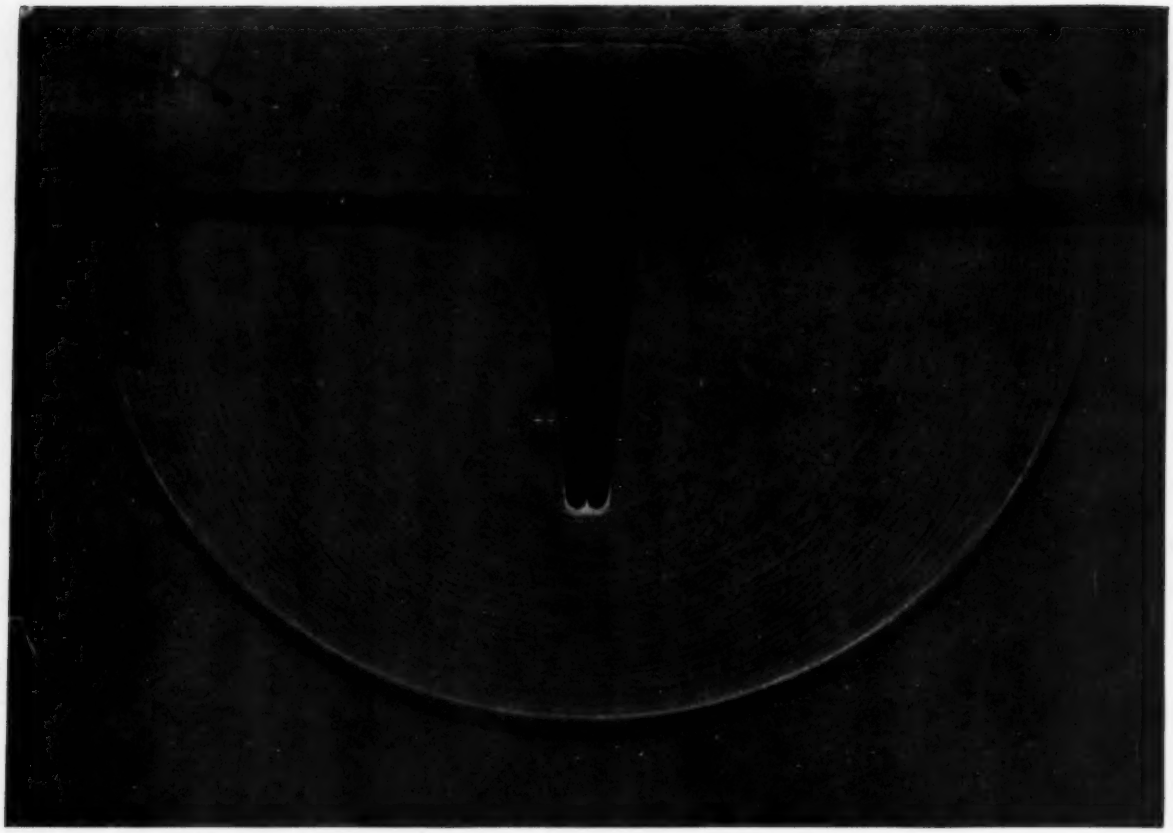

FIG. 2. Spark shadowgram of a wave after advancing 7.8 cm into the water. It was formed by a 4/32" steel sphere having an impact velocity of 3520 ft./sec.

variation as well as sphericity variation was 0.000025 inch; their density was 7.78. These were held in a cylindrical sabot about 16 mm long, split in half longitudinally, and lathe-turned to fit the caliber 30 army standard primed shell. The sabot was made of dowel-pin wood for velocities less than 4000 ft./sec., but for velocities greater than this a "Textalite" plastic sabot was used. The missile was shot from a 30 caliber Winchester smooth-bore test-action rifle. When the missile emerges from the gun, air resistance separates the two halves of the sabot which are stopped by a board with a hole in the center through which the sphere passes. There was nothing about the apparatus that would give the sphere a definite spin, but it was not impossible for the sphere to pick up some rotary motion in its flight. The velocity of each shot was measured just before the sphere hit the surface. The velocity measuring apparatus had an accuracy of about one percent.

DESCRIPTION OF CAVITY AND WAVE

The spark was set off with any time delay up to 20 microseconds after the sphere had struck the surface, catching the wave somewhere between the surface and a point 28 cm below. Since the spheres had subsonic velocities and since they were retarded upon hitting the water, the sphere with its conical cavity lagged behind the wave. Figure 2 shows a wave that has penetrated 7.8 cm. The sphere velocity was 3,520 ft./sec., and it had lost 35 percent of its velocity at the time the shadowgram was taken. The shock wave has a presence-of-light band and an absence-of-light band, the latter being much wider than the one generally observed in air. Its center, as far as can be determined, is at the surface of the water.

The air-filled cavity behind the sphere is opaque to light and casts a sharp silhouette. At the tip of the cavity light is so concentrated

as to form an illuminated cusp. As the sphere slows down, the cusp gradually disappears, and at low velocities became a mere speck of light. The shadow of the ball is not visible in the cavity, but its position can be located by using x-ray shadowgrams. These were taken with a Westinghouse Micronex Surge Generator[7] which produces an x-ray flash of less than a microsecond duration. The flash was produced by discharging á 0.0066-μf condenser at 180,000 volts through a cold-emission x-ray tube. The water tank consisted of a cardboard box containing about 200 cm^3 of water. The true shape of the cavity was also determined since x-rays, unlike rays from the spark, do not refract. Figure 3 shows these two kinds of shadowgrams when a $\frac{6}{32}''$ sphere is shot into water with a velocity of about 2,700 ft./sec. The sphere has penetrated about 3.5 cm in both shadowgrams. By comparing the two pictures one can show that the center of the sphere is at the tip of the cusp. Thus the cusp is formed by light bent around and behind the sphere.

The spark shadow of the cavity in the vicinity of the sphere is wider than the geometrical shadow. In Fig. 3 the width at the level of the center of the sphere is 38 percent wider than the true width as shown in the x-ray. This anomalous width is present for a distance of several sphere diameters up the cavity but in decreasing magnitude. At higher sphere velocities the increase in width is greater; a doubling of the width has been frequently observed.

The concentration of light behind can be explained by the increase in pressure and density around the sphere. The pressure at the nose of the sphere reaches thousands of atmospheres which is sufficient to produce a considerable change in the refractive index. While at present the details of the manner in which these optical effects are produced are not clear, it is hoped that further study will develop a method for determining the pressure distribution around the sphere from measurements made on the cusp and the anomalous width. It is obvious from the refraction effects involved that the analysis must be one that deals with a compressible fluid.

[7] L. F. Ehrke and C. M. Slack, Elec. Eng. **54**, 149 (1935).

WIDTH OF BAND AND PRESSURE

The width of the dark band varies with the pressure in the wave. Hilton[8] has shown that for air the width is bounded by a ray tangent to the wave front and by a ray which suffers a minimum deviation in traversing the medium immediately behind the front. When this is applied to water, the fractional change in refractive index ϵ is given by

$$\epsilon = 0.272 d^{\frac{1}{2}} R^{-\frac{1}{2}} D^{-1}, \qquad (1)$$

where d is the band width, R the radius of curvature of the wave front (as measured in the photograph), and D is the distance from the point of tangency to the photograph.

In deriving Eq. (1) it was assumed that the pressure in the wave was constant over the region immediately behind the wave front. Preliminary measurements with tourmaline crystals have shown that air pressures are not constant but rather rise to a peak and then fall off with what appears to be an exponential decay. The crystal measurements are not precise enough to determine if the peak is sufficiently dull to permit the unqualified use of Eq. (1). However, in this investigation only relative changes in shock wave strength are of interest. Hence an effective $\bar{\epsilon}$ will be calculated which may be considered to be a measure of the peak value for ϵ. In the same manner $\bar{p}$ will be the effective pressure behind the wave.

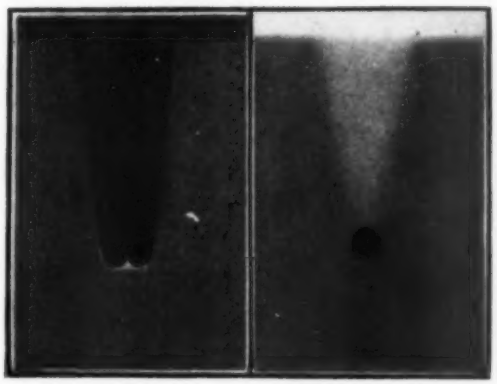

FIG. 3. Comparison of spark shadowgram and an x-ray shadowgram showing the effect of refraction in the spark shadowgram. Spheres of diameter 6/32" and impact velocity of about 2700 ft./sec. were used.

[8] W. F. Hilton, Proc. Roy. Soc. **A169**, 174 (1938).

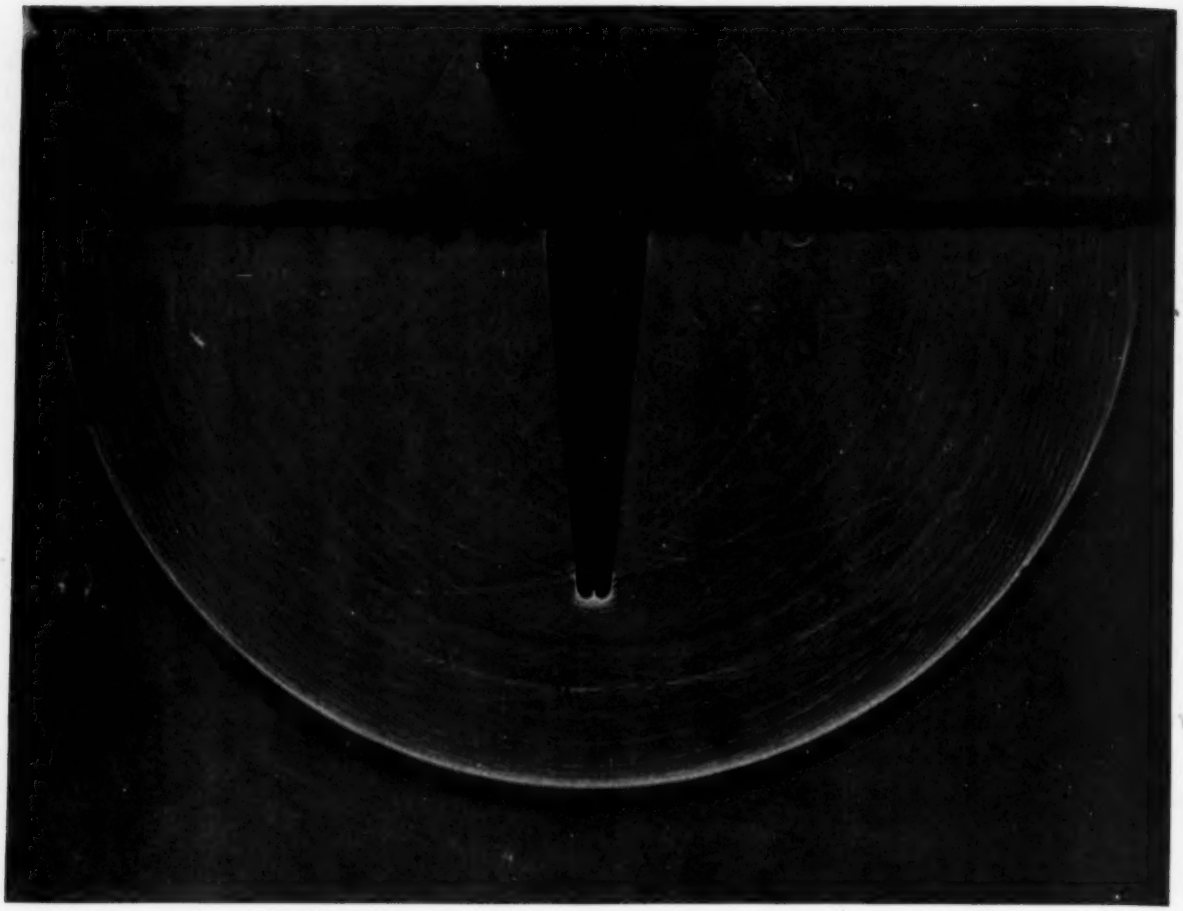

FIG. 4. Spark shadowgram showing variation in band width over shock wave front. Sphere had initial velocity of 4840 ft./sec. and a diameter of 4/32". Shock wave has penetrated 10.7 cm of water.

The next consideration is that of converting the data for ϵ into pressures. Poindexter and Rosen[9] have made a direct determination of this relationship by varying the pressure in a water-filled vessel of optical-prism shape and observing the change in deviation of a spectrum line. For low pressures such as encountered in this experiment they find $\epsilon=1.06\times10^{-5}p$ where p is in kg/cm². The only disadvantage in using this expression is that it conforms to an isothermal change, whereas the change produced by a shock wave is more nearly adiabatic.

A second approach to finding the proper relationship between ϵ and p is that of using density data. For this purpose the Rankine[10]-Hugoniot[11] expression for adiabatic changes across a shock wave can be used. At low pressures and for an adiabatic coefficient $\gamma=7.15$. This gives $\Delta\rho/\rho=4.54\times10^{-5}p$. Also Lyons[12] has shown that Newton's law relating density and

TABLE I. Showing how various theoretical laws and experimental observations give values to k_3 in the relationship $\epsilon=k_3p$. Here $k_3=k_1k_2$, $\epsilon=k_1\Delta\rho/\rho$ and $\Delta\rho/\rho=k_2p$. The pressure p is in kg/cm².

	Bridgman ($k_2=5.06\times10^{-5}$)	Rankine-Hugoniot ($k_2=4.54\times10^{-5}$)
Newton ($k_1=0.219$)	1.11×10^{-5}	0.995×10^{-5}
Lorentz-Lorentz ($k_1=0.276$)	1.40×10^{-5}	1.26×10^{-5}
Poindexter-Lyon	$.610\times10^{-5}$	

[9] F. E. Poindexter and J. S. Rosen, Phys. Rev. **45**, 760 (1943).

[10] Rankine, Phil. Trans. Roy. Soc. **160**, 277 (1870).

[11] H. Hugoniot, Journal de l'École Polytechnique, Paris Cahiers, 57–59 (1887–1889).

[12] W. J. Lyons, J. Opt. Soc. Am. **26**, 144 (1935).

refractive index changes is obeyed for water. It is $\epsilon=0.219\Delta\rho/\rho$. Thus by using Newton's law and the Rankine-Hugoniot adiabatic one obtains $\epsilon=0.995\times10^{-5}p$ which is not significantly different from Poindexter and Rosen's observation.

Two other sources of information in this field are also of interest. One is the static pressure-density determinations of Bridgman,[13] and the other is the Lorentz-Lorentz law relating ϵ and $\Delta\rho/\rho$. These have been put into Table I along with those already discussed. The table is self-explanatory; there is surprisingly little difference in the value of the constants involved when one considers the difference in the methods concerned. In this report 1×10^{-5} was chosen for the constant, it being the average of Poindexter-Rosen determination and the constant calculated from the Newton and Rankine-Hugoniot equations.

DISTRIBUTION OF SHOCK WAVE STRENGTH OVER WAVE FRONT

Because the width of the dark band is related to the strength of the wave, widths were measured under various experimental conditions. It is observed first of all that the width or strength of the wave is not the same over the wave front but is greatest directly ahead of the sphere, and least where the wave touches the surface. In addition to this general observation it is noted that the wave front changes in character at a point which is located about 7° from the surface. This is clearly shown in Fig. 4 where the black band is observed to taper off in width while approaching a point 7° along the arc. Other photographs have shown an abrupt change in the curvature of the wave front at this point, the wave below 7° being nearly parallel and perpendicular to the surface. This abrupt change in the strength of the wave at 7° is probably due to the fact that it is along this radial line that the sphere loses contact with the water during its flight. Measurements of the angle between the equatorial plane and the radial line to the point at which the water leaves the sphere gave a value of 9° 20′ with a probable error of 8′. These measurements were made on $\frac{6}{32}''$ steel spheres by means of x-ray shadowgrams. The spheres had striking velocities of about 3,000 ft./sec. and were measured at penetrations less than 5 cm.

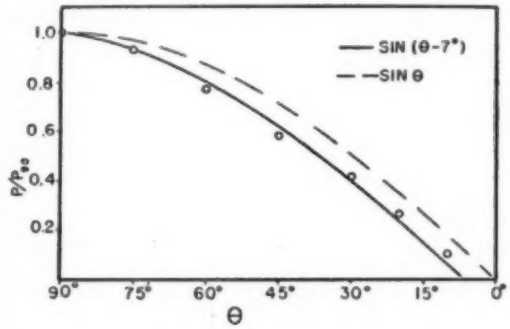

FIG. 5. Showing the angular distribution of pressure over the wave front relative to that straight ahead at $\theta=90°$.

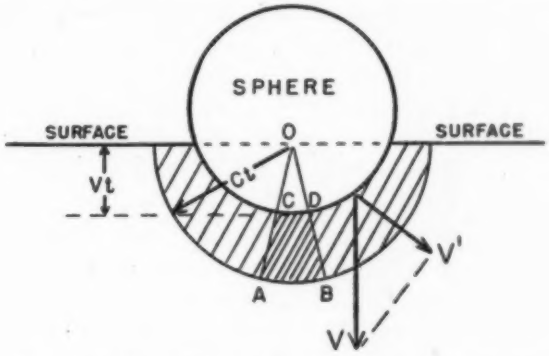

FIG. 6. Schematic sketch showing compressed water volume as sphere enters the water, the compressed volume being trapped between the shock wave front and the sphere.

The width of the dark band was measured for eight different shots, and the average value recorded. To facilitate comparisons all measurements were adjusted for unit width at the 90° position. The sphere velocities varied from 1800 to 4840 ft./sec. and both $\frac{4}{32}''$ and $\frac{6}{32}''$ spheres were used. Since the effective pressure $\bar{p}$ is proportional to $d^{\frac{1}{2}}$ an empirical relationship between $d^{\frac{1}{2}}$ and θ was sought. While it was observed that at angles less than 75° the rate at which the pressure changed with angle was nearly constant, the following expression gave a better agreement at all angles

$$\bar{p}=\bar{p}_{90}\sin(\theta-7). \qquad (2)$$

Here θ is the angle in degrees and $\bar{p}_{90}$ is the pressure directly ahead of the sphere, at $\theta=90°$. The curve for the above expression and the experimental data are shown in Fig. 5.

[13] P. W. Bridgman, Proc. Am. Acad. Sci. 12, 347 (1911).

This falling off in pressure along the shock wave front, as radial lines which are more nearly parallel to the water surface are considered, can be partly understood by making use of Fig. 6 where a drawing of a sphere just entering the water is shown. The arc described by the radius Ct represents the shock wave front. The pressure imparted to the medium is proportional to the velocity of the moving sphere normal to the wave front which in the diagram is represented

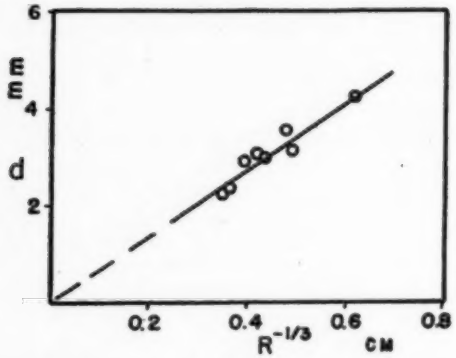

FIG. 7. Showing that the band width is a linear function of $R^{-\frac{1}{3}}$, or that the pressure falls off as R^{-1}. Steel spheres 4/32" in diameter traveling with a velocity of 3600 ft./sec. were used.

by the vector V'. When the sphere enters the water with a velocity close to the velocity of the shock wave, the velocity vector V' is nearly normal to both the wave front and the sphere. Since the above measurements were made on spheres having nearly sonic velocities, one can assume that the velocity and pressure along a radial line designated by θ is approximately proportional to $V \sin \theta$ or simply $\sin \theta$. The curve for $\sin \theta$ is also plotted in Fig. 5, and it is seen that while it has the general shape of the experimental curve its values for the pressures are larger than those found in the experiment.

One of the surprising observations on the angular distribution of the width of the shock wave band comes with the discovery that the distribution changed very little when missiles of quite different shapes were used. Small cylinders striking edge-wise and cones with apex angles equal to 90° produced waves which by inspection resemble those produced by the spheres. This was also true for pieces of wood of irregular shape which occasionally strike the water. Evidently the transfer of momentum to the water cannot be explained entirely in terms of velocity components normal to the missile's surface, as it was above for the sphere.

DECREASE IN SHOCK WAVE STRENGTH WITH DISTANCE

The spark shadowgrams of waves having the same strength show that those that have advanced further into the tank are weakest. This is understandable since the energy per unit volume decreases with the geometrical expansion of the wave front. The energy per unit volume E decreases as R^{-2}. If one neglects changes in the entropy as the wave front expands, then $E = \int p dv$, and at low pressures $dv = -k dp$. It follows that

$$E = (1/2)kp^2 - (1/2)kp_0^2.$$

Neglecting the second term and remembering that E is proportional to R^{-2}, one obtains

$$p = k'R^{-1};$$
$$d = k''R^{-1}.$$

Thus while the pressure falls off fast with increasing R, the width decreases relatively little. This difference arises from the fact that an increase in radius of the spherical wave front also increases the deviation of the minimum ray.

To test this pressure-distance relationship, band widths were measured at penetration depths ranging from 4.25 to 21.95 cm. To obtain the photographs of penetrations near 20 cm, the spark was lowered below its original water level position so that the corrections on D and d, due to the geometry of the apparatus, became negligible. Since the spheres did not all have the same velocity, the band width was reduced to correspond to a band width at a velocity of 3600 ft./sec.; experimental data described in a succeeding section was used for this. The test was carried out with a $\frac{4}{32}$" steel sphere, and the band width was measured at the 90° position on the arc. The results are shown in Fig. 7 where d is plotted against $R^{-\frac{1}{3}}$. The linearity of the plotted points shows that the effective pressure in the shock wave falls off according to R^{-1}. Unfortunately the width is such a slowly varying function of R that small deviations from the R^{-1} law would not be observed in this experiment. It is not possible, for example, to observe the effect

of changes in the entropy which may accompany the expanding wave.

VARIATION OF WAVE VELOCITY WITH PRESSURE

When the high pressure shock waves are examined it is seen that the wave front does not describe a perfect arc of a circle but is elongated in the direction of the missile's flight, forming an ellipse of small eccentricity. The wave front in line with the sphere's trajectory is stronger and travels with greater speed while the wave near the surface travels with sonic velocity. The eccentricity is so small that it can only be measured for spheres traveling with velocities around 4000 ft./sec. or larger.

Measurements on four plates gave percentage differences $\Delta R/R$ between the long and short axis of the elliptical wave front ranging from 1.9 to 4.3 percent. This is interpreted as meaning that the average wave velocity in the strong portion of the front was from 1.9 to 4.3 percent faster than the velocity of sound in water. These data are collected in Table II. In the fourth column the average Mach number which the wave possesses during its flight is recorded; the Mach number is the ratio of wave to sound velocity, and it is continually decreasing as the wave expands and weakens.

That shock wave velocity depends on its strength is well known.[1] If the velocity of a plane shock wave is C and the velocity of the medium is u, then the conservation of mass across the wave front requires that

$$\rho_0 C=\rho(C-u). \tag{3}$$

The momentum imparted to the water equals the pressure difference so that

$$p-p_0=\rho_0 C u. \tag{4}$$

Eliminating u from the above gives for the velocity of the wave

$$C^2=\rho(p-p_0)/((\rho-\rho_0)\rho_0). \tag{5}$$

When the conservation of energy is taken into account and Tammann's[14] equation of state,

$$(p+3000)v=KT,$$

is used, a relationship between p, p_0, ρ and ρ_0 is found; this is the well-known Rankine[10]-Hugoniot[11] equation

$$\frac{\rho_0}{\rho}=\frac{(\gamma+1)P+(\gamma-1)}{(\gamma-1)P+(\gamma+1)}, \tag{6}$$

where $\gamma=7.15$ and is the adiabatic constant, and $P=(3001)/(p+3000)$. The pressure p is in atmospheres.

By making use of (6) and (5), pressures corresponding to the Mach numbers observed above were calculated. These are recorded in Table II along with pressures calculated from the band width at the forward portion of the wave. It is observed that the average pressure in the wave during flight as measured from the ellipticity of the wave front is larger than that calculated from the band width. This is as it should be, since the band width measurement gives the final pressure only. While it would be interesting to calculate the final pressure in terms of the average pressure and thus correlate it with the pressure obtained from band widths, two factors make it inadvisable. One of these is the experimental difficulty entailed in measuring the eccentricity of the elliptical wave front; the other is the difficulty in knowing how the pressure varies with R at the limit, when R is zero or comparable with the sphere diameter.

TABLE II. Average Mach numbers for several wave fronts as determined from the eccentricity of the wave. Also a comparison of pressure in wave measured from band width and from average Mach number.

V ft./sec.	R cm	$\Delta R/R$	Average Mach number	Pressure kg/cm² From Mach number	From width of band
4,730	9.8	0.043	1.043	462	137
4,840	11.8	0.034	1.034	371	141
4,480	12.13	0.031	1.031	337	102
4,090	9.45	0.019	1.019	205	95

VARIATION OF SHOCK WAVE PRESSURE WITH IMPACT VELOCITY

Inspection of the shadowgrams shows that the band width becomes larger as the impact velocity of the sphere is increased. The difference in width can be seen in Fig. 8 where a shadowgram for a $\frac{4}{32}$" sphere having a velocity of 1830 ft./sec. is shown; this may be contrasted with Fig. 4,

[14] G. Tammann, Ann. d. Physik **37**, 975 (1912).

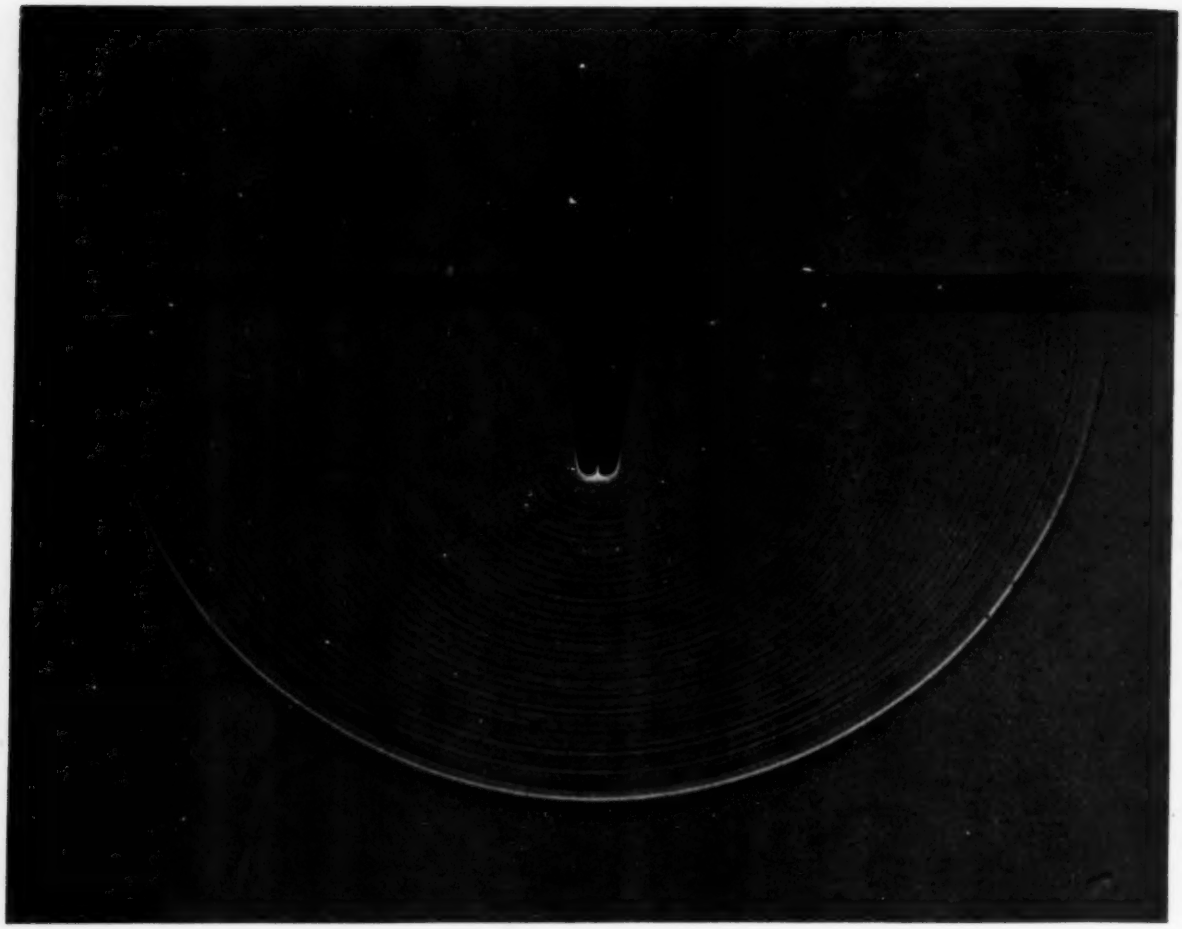

FIG. 8. Spark shadowgram of shock wave produced by a low velocity sphere. The 4/32" steel sphere had an initial velocity of 1830 ft./sec. Shock wave has penetrated 6.5 cm of water.

showing a wave formed by the same sized sphere traveling with a velocity of 4840 ft./sec. A series of seventeen shots were made at different velocities to determine just what relationship does exist between pressure and impact velocity. The $\frac{4}{32}$" steel spheres were used, and the velocities ranged from 1830 to 4840 ft./sec.; the latter is just above the velocity of sound in water. All measurements were made at $\theta=90°$, that is, at the foremost point of the wave.

The spark was triggered so that the wave was shadowgraphed as close to a 10-cm penetration as possible; all measured waves fell between 7.0 and 15.2 cm. The width was measured with a vernier caliper with an accuracy which was estimated to be ± 0.01 cm. All widths were reduced to correspond to a wave penetration of 10 cm by making use of the already established fact that the width varies as $R^{-\frac{1}{4}}$. The widths were further reduced to correspond to $D=17.2$ cm for those shots which did not follow the aim of the gun. The spheres rarely strayed more than a centimeter from the central position. Still another correction consisted of one for the refraction of the diverging rays as they passed from the water to the air. The data are plotted in Fig. 9.

By making use of Eq. (1) these widths were employed to calculate the effective index change $\bar{\epsilon}$ and effective pressure $\bar{p}$ at the front of the shock wave. The data are recorded in the logarithm plot of Fig. 10. The points are observed to fall on a straight line having a slope 2.17. The data conform to the empirical relationship

$$\epsilon=6.07\times 10^{-4}V^{2.17}, \tag{7}$$

where V is the impact velocity in kilometers per second. The corresponding expression for effective pressure is

$$p = 607\, V^{2.17} R^{-1}, \tag{8}$$

where V is in kilometers per second, R in cm and p in kg/cm². It is to be remembered that the above formula applies only to a $\frac{4}{32}''$ steel sphere.

The increase in pressure with sphere velocity can be partially explained by making certain simplifying assumptions regarding the events which occur at entry. It is assumed first of all that the compressible water is trapped between the shock wave front and the sphere entering the water. It is also supposed that part of the water escapes in the splash so that the trapped volume is smaller than at first supposed.

Let the sphere be in the process of entering the water as shown in Fig. 6. The compressed region is contained between the sphere and the wave front of radius, Ct, where C is the wave velocity and t a small time interval. During this same time interval the sphere advances a distance Vt.

In the cone OAB (the pressure within which determines the pressure at the center of the wave front) the volume is reduced to $ABCD$. The new density ρ is given by

$$\frac{\rho_0}{\rho} = \frac{(Ct)^3 - s(Vt)^3}{(Ct)^3}, \tag{9}$$

where ρ_0 is the original density of the water, and s represents that fraction of water volume swept out by the sphere which is not lost in the splash.

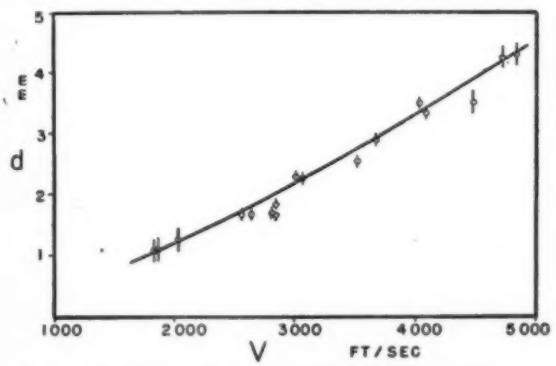

FIG. 9. Showing how band width at the forward portion of the wave varies with impact velocity; 4/32″ steel spheres. The length of vertical dashes indicates estimated error in measuring the bands. $R=10$ cm, $D=17.2$ cm.

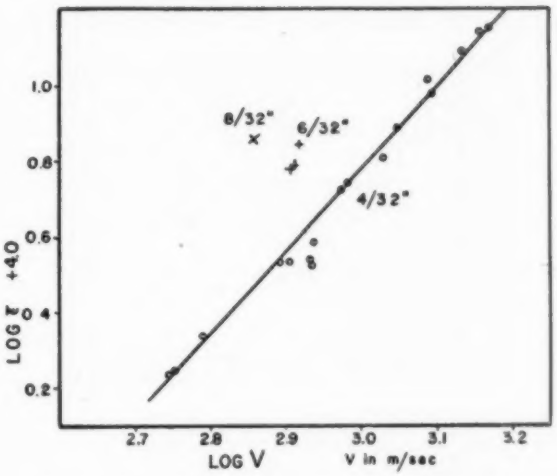

FIG. 10. Showing a logarithmic plot of effective refractive index and effective pressure as a function of sphere velocity; 4/32″ steel sphere, $\theta=90°$, $R=10$ cm.

The above reduces to

$$\rho_0/\rho = 1 - s(V/C)^3.$$

A fair agreement with the experimental data is obtained by setting $s=0.25$; this calls for a large loss of water when it is compared to the volume of the sphere, but in absolute magnitude it is quite small.

The pressures equivalent to the density ratios calculated from the above were obtained from the Rankine-Hugoniot Eq. (6). After the pressures were calculated for various sphere velocities they were reduced to a wave position of 10 cm. In this reduction use was made of the observation that the pressure in the wave falls off inversely as the first power of the distance. Since it was necessary to assume a value for the radial distance at which the wave was created, a distance equal to the sphere diameter was chosen.

The calculated pressure-curve and the experimental data are shown in Fig. 11. One observes that the calculated pressure increases with velocity and agrees in absolute magnitude near a velocity of 2500 ft./sec. At velocities approaching the velocity of sound in water, however, the calculated pressures deviate considerably from those observed experimentally. For a treatment of this problem at high velocities a more detailed analysis of the volume of water lost in the splash is called for.

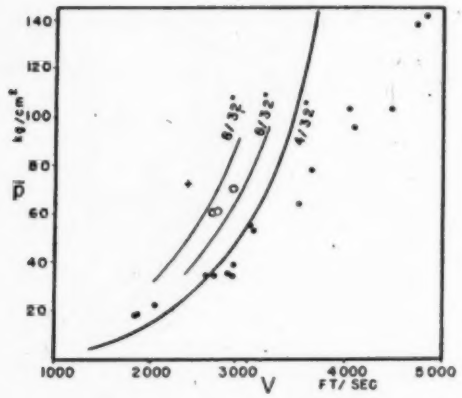

FIG. 11. Showing measured pressures (points) of wave as a function of velocity; $R=10$ cm, $\theta=90°$. The curve is the calculated pressure based on a loss of water in the splash and the Rankine-Hugoniot compression law. It was assumed that the wave originated at a point below the surface which was equal to the diameter of the sphere.

WAVE STRENGTH VARIATION WITH PROJECTION AREA AND DENSITY

Shock wave patterns from a great variety of missiles have been observed. These include small specks of wire from the trigger screen with areas less than a 0.002 cm² and pieces of wood (parts of the sabot) having areas of about 1.0 cm². It is clear from inspecting these shadowgrams that the missiles having large projection areas produce the widest bands.

To find the relationship between projection area and shock wave strength, shadowgrams were made with $\frac{4}{32}''$, $\frac{6}{32}''$, and $\frac{8}{32}''$ spheres. The width at the 90° position along the arc was then measured. This width was then corrected and reduced according to the methods described in the previous section. Log $\bar{\epsilon}$ values for the data of the $\frac{6}{32}''$ and $\frac{8}{32}''$ spheres were inserted in the graph of Fig. 10. There was only one point for the $\frac{8}{32}''$ sphere; since it was found, while acquiring this datum, that an $\frac{8}{32}''$ sphere breaks the tank.

Lines were drawn through the experimental points in Fig. 10 which were parallel to the line for the $\frac{4}{32}''$ sphere. From the intercepts the constant appearing in Eq. (8) was determined for the $\frac{6}{32}''$ and $\frac{8}{32}''$ sphere. When these are plotted against projection area of the sphere as they are in Fig. 12, a linear relationship is found. Thus the pressure in a shock wave increases linearly with the sphere's projection area A. The pressure is given by the formula

$$\bar{p}=(300+3920A)\,V^{2.17}R^{-1},$$

where R is in cm, V in kilometers/sec., A in cm and $\bar{p}$ in kg/cm².

A study was made of the effect of sphere density on the strength of the shock waves. A comparison was made of the band width and pressure when the wave was produced by aluminum and steel spheres. The aluminum spheres were 0.277 times lighter than those of steel. The velocity for all shots were kept nearly the same, the average being 2870 ft./sec.; $\frac{4}{32}''$ spheres were used throughout. It was found that the wire-screen trigger could not be used to trigger the aluminum sphere, since the wire cut the aluminum and destroyed its sphericity. A microphonic trigger was used in place of it. This consisted of a carbon microphone and amplifier which fed into the delay circuit.

The spark shadowgraphs showed no apparent difference between the bands formed by the aluminum spheres and those of steel. The data are collected in Table III where the pressures for two aluminum shots relative to those of steel are given. The density ratio is also given for comparison. The pressure that was used for the steel sphere was an average of three shots. One observes that there is no appreciable difference in the pressures even though the density change is about threefold. This lack of importance on the part of density is frequently observed in the spark shadowgraphs when fragments of the wooden-sabot accompany the sphere through the

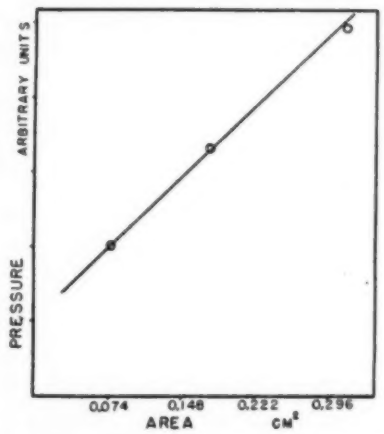

FIG. 12. Showing how the shock wave pressure increases linearly with the projection area of the sphere.

sabot catcher and also strike the water. They produce a very wide band in spite of their small density.

These observations of the effect of sphere size on the strength of the shock wave can be explained, in part, by referring to the model of the impact-action which was introduced in the previous section. In this model two arbitrary parameters were introduced; one was the coefficient representing the loss of water by splash, while the other was the distance below the surface at which the wave was considered to be formed.

One observes, first of all, that an analysis based on the model is independent of density which is in agreement with the experiment. Likewise the model calls for an increase in pressure with projection area as was also observed; however, the rate of increase is different. For the model the pressure increases as $A^{\frac{1}{2}}$ while it was observed to increase proportional to (constant$+A$). The calculated and measured pressures, as they depend on A, are plotted in Fig. 11. The calculated values are too small, showing that a more rigorous treatment than the one furnished by this simple model is needed.

TABLE III. Comparison of shock wave pressure for aluminum and steel spheres. Diameter = 4/32", V = 2870 ft./sec.

Exp. no.	$\bar{p}_{Al}/\bar{p}_{Fe}$	ρ_{Al}/ρ_{Fe}
64	1.08	0.277
59	1.03	

ACKNOWLEDGMENTS

The author is pleased to acknowledge his appreciation to Dr. E. Newton Harvey for suggesting this investigation and for the many stimulating discussions which accompanied it. He also wishes to thank Mr. Harold Towne and Mr. James Hay for their help in obtaining the experimental data.

Erratum: Refraction Effects in Electron Diffraction

LORENZO STURKEY AND LUDO K. FREVEL
The Dow Chemical Company, Midland, Michigan

[Phys. Rev. **68**, 56L (1945)]

AN error was made in the equation included for δ, the deviation of diffraction angle from the Bragg angle. The correct form should be:

$$\delta = (\pm[\tan r_1] \pm [\tan r_2])(P/2E).$$

PHYSICAL REVIEW VOLUME 68, NUMBERS 9 AND 10 NOVEMBER 1 AND 15, 1945

Values of the Optical Constants for Beryllium, Magnesium, and Zinc

ROBERT O. BOCK*
Department of Physics, Cornell University, Ithaca, New York
(Received September 10, 1945)

Reflectivities of evaporated metal films have been observed under varying conditions, allowing the computation of conductivities and dielectric constants by a previously described method. A reflectometer employing both a photo-cell and a thermopile permitted measurements in the visible and near infra-red regions. Curves are included showing the values of the constants for beryllium, magnesium, zinc, and copper. Comparisons are made with other published results.

PREVIOUS investigations of the optical constants of metals have for the most part been limited in frequency range by the nature of the methods of measurement. A second common drawback has been the questionable nature of the metallic surfaces employed, since mechanically polished bulk metals or very thin films (the properties of which are not truly characteristic of bulk material) have generally been used. The present investigation has sought to avoid these difficulties. The method of measurement employed has been described in detail elsewhere.[1]

Though the actual optical quantities determined are usually the index of refraction n and the extinction coefficient k (both as functions of frequency), the modern theory of solids interprets more directly the conductivity for frequency $\nu(=\sigma_r=nk)$ and the dielectric constant for frequency $\nu(=\epsilon_r=n^2-k^2)$. These significant quantities are found directly in the method employed and, plotted as functions of frequency, give information concerning the nature of the electronic energy bands in the solid state.[2]

The measurement of reflectivities, which is the basis of the method employed here, is effected as readily in the infra-red region of the spectrum as in the visible and ultraviolet regions. For this reason the spectral range chosen was that extending from $\lambda=4800$A to $\lambda=24{,}000$A; this allows observations in a new range of frequencies as well as comparison with results obtained by other methods in the visible region. The arrangement of apparatus used is shown in Fig. 1. The image of an incandescent light source is thrown upon the entrance slit (S_1) of a monochromator; the collimating mirror M_1 is an off-axis parabola which reflects light in a homogeneous beam to the constant deviation prism P, from which light proceeds to M_2 (a duplicate of M_1) to be refocused in a slit image at S_2, the exit slit of the monochromator. The radiation is recollimated (L_1) in the reflectometer, polarized by the Nicol prism N, and reflected by the metallic mirror on which measurements are being made (MM); the reflected intensity is observed by the photo-cell or thermopile (T). The apparatus may be set to measure the intensity of the incident radiation, or that for radiation reflected at angles of incidence of 80°, 70°, 60°, or 50°.

Some guidance in the choice of metals for measurements was furnished by the theorists' picture of the solid state, which portrays energy bands for divalent metals as overlapping one another more than for monovalent or trivalent materials. This results in smaller energy differences for the transitions which may be observed; the first anomalous absorption peak for monovalent materials is usually in the ultraviolet

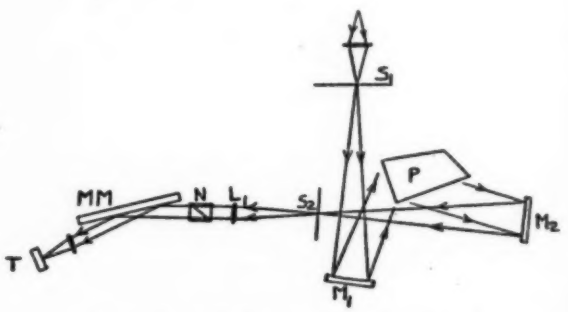

FIG. 1. Optical system employed for reflectivity measurements.

* Now at Arma Corporation, Brooklyn, New York.
[1] J. R. Collins and R. O. Bock, Rev. Sci. Inst. **14**, 135 (1943).
[2] See, for example, F. Seitz, *Modern Theory of Solids*.

region, whereas this occurs in the near infra-red for most divalent metals. Measurements were made on magnesium, beryllium, zinc and, in testing apparatus, copper.

Evaporation technique was employed in the preparation of the metallic surfaces. Accepted methods were used, the metal sources being heated in vacuum by electric currents in tungsten coils or troughs. The $1\frac{1}{2}''\times 6''$ plate glass blanks upon which the films were deposited were tested for flatness, cleaned thoroughly, and mounted at a distance of 10 to 15 cm from the source of evaporated metal. A vacuum of about 10^{-6} millimeter of mercury was maintained. Evaporation was carried on until the mirrors appeared "opaque" to a bright incandescent light.

The accuracy and reliability of results depend upon the nature of the material deposited as regards oxidation and ease of deposition (repeatability) of the films. A second and perhaps more important factor is the nature of the graphical intersections obtained in the method of reducing the data.[1]

RESULTS

Beryllium (Fig. 2)

The samples of beryllium used were 99.9 percent pure and formed durable, easily duplicated films at an evaporating temperature of about 1400°C. Figures for the estimated probable errors in σ and ϵ (Table I) are arrived at as follows: determine a probable error in measurement of reflectivity (0.8 percent was the figure used here), apply this difference arbitrarily to some value obtained for reflectivity and observe the change introduced in the values of σ and ϵ in reducing the data. (Note that this does not take into account possible systematic errors in the nature of the films used.)

TABLE I. Errors in constants for beryllium.

$\bar{\nu}$ (cm^{-1})	Error in ϵ	Error in σ
2.22×10^{4}	0.14	0.13×10^{15}
0.833	0.32	0.12
0.526	2.1	0.12
0.476	6.4	0.27

The results, shown in Fig. 2, agree very well with those obtained by Givens[3] in the frequency range covered by both observers. Differences in the conductivity are of the order of a few percent, but are somewhat larger for the dielectric constant.

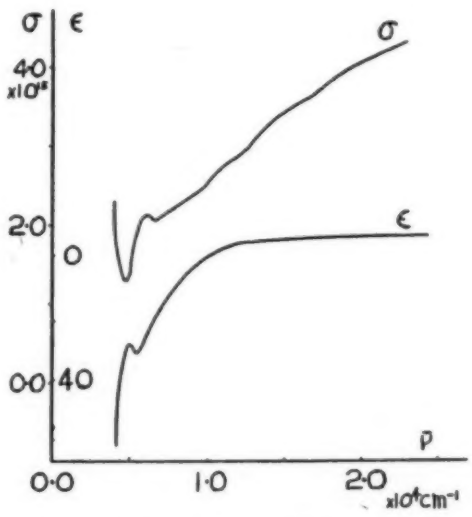

FIG. 2. Conductivity and dielectric constant *vs.* wave number for beryllium.

Magnesium (Fig. 3)

Impurities in the magnesium used totaled about 0.07 percent. The material was readily evaporated, but duplication of the films was not easy since oxidation begins at once upon exposure to air. This fact throws a little uncertainty on the results in addition to the errors shown (Table II).

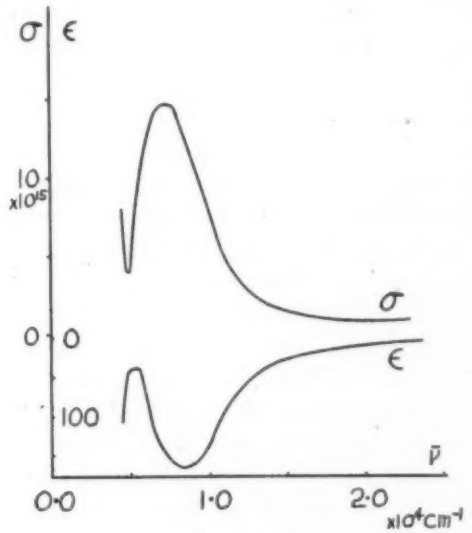

FIG. 3. Conductivity and dielectric constant *vs.* wave number for magnesium.

[3] M. P. Givens, Phys. Rev. **61**, 626 (1942).

TABLE II. Errors in constants for magnesium.

$\bar{\nu}$ (cm^{-1})	Error in ϵ	Error in σ
2.22×10^{4}	1.8	0.11×10^{15}
1.67	1.4	0.12
1.33	2.0	0.18
1.11	38.0	1.9
0.667	27.0	5.6
0.625	11.0	3.2
0.571	2.4	2.1
0.500	1.6	0.45
0.465	11.0	0.96

No previous results are available for comparison. It is thought that the large peak in conductivity at $\bar{\nu}=0.7\times10^{4}$ cm^{-1} represents the first anomalous absorption.

Zinc (Fig. 4)

Zinc of Kahlbaum purity was evaporated readily upon a thin layer of chromium, since this technique diminishes the haziness which tends to characterize the zinc surface.[4] Deterioration is slow, and repeated attempts on new films showed practically identical results (Table III).

The flattening of the curve for the dielectric constant at the low frequency limit of the work makes another absorption peak appear likely in the infra-red. It should be born in mind, however, that this occurs in a part of the spectrum where the accuracy of the work is not great.

An interesting comparison exists between these results and those of Bor, Hobson, and Wood,[5] who used polished bulk zinc. Their conductivity curve resembles this one in shape, the principle peaks being about 0.07×10^{4} cm^{-1} apart for both observers. The absolute value of the conductivity reported here (in the region of the peak) is only about half that found by Bor, Hobson, and Wood, but it is worth noting that lower values of conductivity generally result when amorphous surface layers on a metal have been reduced.[6]

The separation of the p and s bands in a metal tends to increase with atomic number. The first anomalous absorption peak generally represents a transition between these bands, hence the peak should shift toward the ultraviolet as the atomic number increases. This

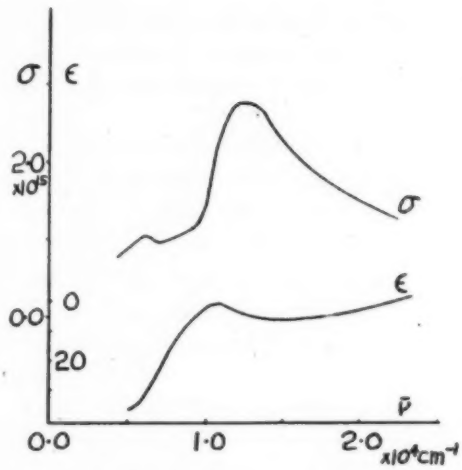

FIG. 4. Conductivity and dielectric constant *vs.* wave number for zinc.

TABLE III. Errors in constants for zinc.

$\bar{\nu}$ (cm^{-1})	Error in ϵ	Error in σ
2.08×10^{4}	0.093	0.029×10^{15}
1.56	0.21	0.089
1.11	0.20	0.070
0.910	0.24	0.054
0.625	3.7	0.12

behavior is roughly indicated by the magnesium and zinc curves, where the peaks appear at $\bar{\nu}=0.75\times10^{4}$ cm^{-1} and at $\bar{\nu}=1.27\times10^{4}$ cm^{-1}, respectively. The accompanying data for beryllium do not verify this shift. A further measurement was sought for cadmium, but the experimental difficulties encountered in the preparation of the film have postponed the work. A preliminary rough observation by Collins has indicated a peak somewhere in the vicinity of that found for zinc.

Copper (Fig. 5)

A high grade of copper was used, the total of impurities being about 0.01 percent. Though evaporation proceeds readily enough, the resulting films are extremely sensitive in their characteristics to the pressure maintained in the chamber, the cleanliness of the glass blank and apparently to a few other unknown conditions. Deterioration of the resulting film is very rapid, and much care must be exercised in obtaining readings. In most of the spectral range covered here, the experimental errors are very large (Table IV).

[4] G. B. Sabine, Phys. Rev. **55**, 1064 (1939).
[5] J. Bor, A. Hobson, and C. Wood, Proc. Phys. Soc. **51**, 932 (1939).
[6] Mott and Jones, *Properties of Metals and Alloys*, p. 118.

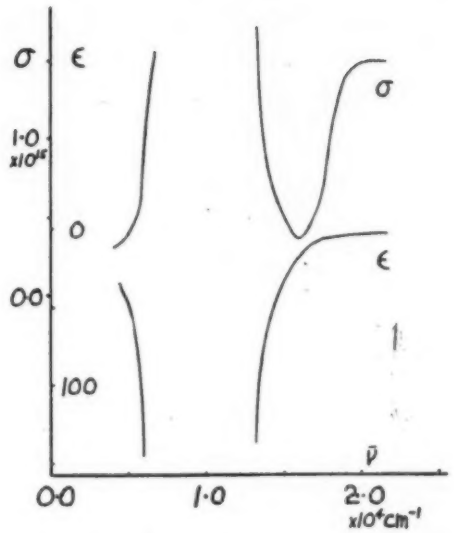

FIG. 5. Conductivity and dielectric constant *vs.* wave number for copper.

Many sets of values have been published for copper. Among the more recent are those of Lowery, Bor, and Wilkinson,[7] who used lightly polished surfaces in order to minimize the formation of small crystals and amorphous layers. They obtained conductivities in the frequency range $\bar{\nu}=2.08\times10^4$ cm^{-1} to $\bar{\nu}=1.67\times10^4$ cm^{-1} which agree almost identically with the values obtained here. Numerous other workers have reported similar shapes to the curves though the quantitative agreement is not so striking. Givens[3] does not observe this absorption, believing the peak usually reported to be due to copper oxide. While the data here are not on the same films used by Givens, extreme caution was exercised to duplicate as nearly as possible the films employed in his measurements. The discrepancy is unexplained.

TABLE IV. Errors in constants for copper.

$\bar{\nu}$ (cm^{-1})	Errors in ϵ	Errors in σ
2.08×10^4	0.14	0.060×10^{15}
1.85	0.16	0.035
1.60	5.2	0.10
1.43	23.0	0.32
0.476	12.0	0.12

In conclusion, the author wishes to express his gratitude to Professor J. R. Collins for his suggestion of the problem and his constant help and encouragement throughout the work; and to Professor D. H. Tomboulian for his aid and advice in the preparation of the evaporated metal films.

[7] Lowery, Bor, and Wilkinson, Phil. Mag. **20**, 390 (1939).

Erratum: A Generalization of the Dielectric Ellipsoid Problem

R. CLARK JONES
Polaroid Corporation, Cambridge, Massachusetts
[Phys. Rev. **68**, 93 (1945)]

THE symbols used in the article are somewhat confusing, inasmuch as there is only a slight correlation between the font of the symbol and the type of physical quantity which it represents. The symbols **E**, **P**, **r**, and **i** represent vectors, and the symbols $\boldsymbol{\epsilon}$, $\boldsymbol{\varepsilon}$, $\boldsymbol{\sigma}$, $\boldsymbol{\alpha}$, $\boldsymbol{A}$, $\boldsymbol{B}$, and $\boldsymbol{T}$ represent tensors.

Equations (13) and (16) should be printed as follows:

$$\mathbf{P}_e=\frac{\varepsilon_1-1}{4\pi}\mathbf{E}_1, \tag{13}$$

$$\mathbf{P}=\mathbf{P}_e+\mathbf{P}_\sigma=\frac{\varepsilon_1-1}{4\pi}\mathbf{E}_1. \tag{16}$$

Editor's Note.—Difficulties in obtaining distinctive type and errors made in the editorial offices account for the confusing notations and typographical errors in the original article. For these the author is not responsible.

PHYSICAL REVIEW VOLUME 68, NUMBERS 9 AND 10 NOVEMBER 1 AND 15, 1945

On the Interaction of Radiation and Matter

PETER HAVAS
Pupin Physics Laboratories, Columbia University, New York, New York†*
(Received February 17, 1945)

The quantum theory of radiation describes the effect of retardation in the interaction of two charged particles by the mutual emission and absorption of light quanta. The method used in a previous paper on the interaction of radiation and two particles is extended and applied to a process involving the interaction of any number of charged particles (obeying Dirac's equation) and light quanta. It is shown that in the usual first-order approximation of perturbation theory the resulting expression for the interaction of two free particles obtained by summing over all the intermediate states involving virtual quanta is of the same form for any process. By carrying the summation one step further it is shown that this expression reduces to Møller's formula. The results are relativistically invariant in spite of the usual omission of divergent terms in the Hamiltonian.

I. INTRODUCTION

IT is well known that quantum theory describes a system of charged particles obeying Dirac's equation and the radiation field by a Schrödinger equation[1]

$$H\psi = -i\hbar(\partial\psi/\partial t), \tag{1}$$

whose Hamiltonian can be written

$$H = H_p + H_r + H_s + H', \tag{2a}$$

where H_p represents the Hamiltonian of the particles, H_r that of the light quanta, H_s the electrostatic energy of the particles, and H' the interaction of the particles and the field. We have

$$H_s = \tfrac{1}{2}\sum e_i e_k / r_{ik} \tag{2b}$$

and

$$H' = -\sum e_k(\boldsymbol{\alpha}_k \cdot \mathbf{A}(k)), \tag{2c}$$

where e_k is the charge and $\boldsymbol{\alpha}_k$ the Dirac matrix for the kth particle, $\mathbf{A}(k)$ the vector potential evaluated at the position of e_k, and r_{ik} the distance between the ith and kth particles.

It is not possible with the present methods to solve Eq. (1) with the Hamiltonian (2a) directly. An approximate method often used treats the terms (2b) and (2c) for the interaction as small perturbations causing transitions from a state E_0 with a certain energy and momentum of the particles and a certain number of light quanta to another state E_F. The transition probability is zero unless the total energy is conserved, and then it is given by the well-known equation[2]

$$w_{E_0E_F} = (2\pi/\hbar)\rho_{E_0}|H'_{E_0E_F}|^2, \tag{3a}$$

where ρ_{E_0} is the density of the final or initial states with energy E_0, and

$$H'_{E_0E_F} = \int \psi_0^*(H_S + H')\psi_F d\tau, \tag{3b}$$

is the matrix element for the transition. If we have *free* particles only, the momentum is conserved in this transition too.

If the matrix element for the direct transition is zero, we have to use a succession of simple transitions leading from the initial to the final state through a number of intermediate states, for which we still have conservation of momentum, but no longer conservation of energy. We then have to replace (3b) by

$$H' = \sum \frac{H'_{0,1}H'_{1,2}\cdots H'_{F-2,F-1}H'_{F-1,F}}{(E_0-E_1)(E_0-E_2)\cdots \times(E_0-E_{F-2})(E_0-E_{F-1})}, \tag{3c}$$

where the denominator contains the products of the differences of the energies of the initial and intermediate states, and the numerator the products of the matrix elements for the successive transitions. The sum is over all possible successions of transitions, the choice of which will be discussed in detail later. At this point we note only that it has to be done in such a way

* Publication assisted by the Ernest Kempton Adams Fund for Physical Research of Columbia University.
† Now at Cornell University, Ithaca, New York.
[1] For the general theory and the notation used see W. Heitler, *The Quantum Theory of Radiation* (Oxford University Press, Oxford, 1936), Chapter III.
[2] W. Heitler, reference 1, p. 90.

that the total expression (3c) is of the lowest possible order in the electronic charge e for which it does not vanish,[3] but that otherwise we have to sum over all possible successions.

Equation (2a) contains an explicit expression for the instantaneous Coulomb interaction only, as given by (2b). The matrix element corresponding to (2b) is equal to

$$(4\pi\hbar^2c^2e_1e_2/|\Delta\mathbf{p}|^2)(u_1^{n*}u_1^{n+1})(u_2^{M*}u_2^{M+1}), \quad (4a)$$

for two free particles with Dirac amplitudes u. The effect of retardation is included in H' and is described by the mutual emission and absorption of light quanta. The matrix element corresponding to (2c) and describing the emission or absorption of just one light quantum is given by

$$-e(2\pi\hbar^2c^2/k_\lambda)^{\frac{1}{2}}(u_a^*\alpha_{k_\lambda}u_b). \quad (4b)$$

Here α_{k_λ} is the component of $\boldsymbol{\alpha}$ in the direction of polarization of the light quantum with energy k_λ. For transitions involving more than one quantum (3b) vanishes.

In the simplest possible case of retarded interaction of just two particles in the absence of radiation the retardation is described by the emission of just one virtual quantum by one particle and reabsorption by the other and *vice versa*.[4] In the general case the retardation corresponds to emissions and absorptions described by a large number of terms involving virtual quanta. However it has been shown in a previous paper[5] that for any process involving just two particles, but an arbitrary number of light quanta, we can replace the matrix element for the instantaneous Coulomb interaction (4a) by a 'matrix element for the retarded interaction'

$$\frac{4\pi\hbar^2c^2e_1e_2}{|\Delta\mathbf{p}|^2-(\Delta E)^2}\Big\{(u_1^{n*}u_1^{n+1})(u_2^{M*}u_2^{M+1})-(u_1^{n*}\boldsymbol{\alpha}u_1^{n+1})\cdot(u_2^{M*}\boldsymbol{\alpha}u_2^{M+1}) + \frac{-(\Delta E)^2(u_1^{n*}u_1^{n+1})(u_2^{M*}u_2^{M+1})+(u_1^{n*}\boldsymbol{\alpha}\Delta\mathbf{p}u_1^{n+1})(u_2^{M*}\boldsymbol{\alpha}\Delta\mathbf{p}u_2^{M+1})}{|\Delta\mathbf{p}|^2}\Big\}. \quad (4c)$$

Here $\Delta\mathbf{p}$ is the change in momentum caused by the interaction of the two particles. If $\Delta\mathbf{p}$ is expressed in terms of the initial and final momenta, then the energy difference ΔE is obtained from the corresponding terms of the initial and final energies of the particles and light quanta of the entire process (*not* just of the particular transition involving the two particles).

In the present paper we shall first show that expression (4c) remains valid for processes involving any number of particles and can therefore be used as a matrix element for the retarded interaction of two free particles. This expression was obtained by summing over all the intermediate states involving virtual quanta, but otherwise corresponding to a definite succession of intermediate states for each individual particle. By carrying the summation one step further and considering other successions of intermediate states, we shall furthermore show that the last term of (4c) cancels with other terms of the matrix element. Therefore we can equally well simply use the expression

$$\frac{4\pi\hbar^2c^2e_1e_2}{|\Delta\mathbf{p}|^2-(\Delta E)^2}\{(u_1^{n*}u_1^{n+1})(u_2^{M*}u_2^{M+1}) -(u_1^{n*}\boldsymbol{\alpha}u_1^{n+1})\cdot(u_2^{M}\boldsymbol{\alpha}u_2^{M+1})\} \quad (4d)$$

as the matrix element for the retarded interaction in any process regardless of the number of particles and quanta participating. Expression (4d) is identical with the expression obtained by Møller for a process involving two particles only.[4]

II. THE INTERMEDIATE STATES

We now consider a process involving $z+Z$ light quanta and n particles. Then the conservation of energy and momentum requires

$$E_0=E_1^0+E_2^0+\cdots+E_n^0+a+b +\cdots+z+A+B+\cdots+Z =E_1^F+E_2^F+\cdots+E_n^F=E_F \quad (5)$$

[3] It is a well-known difficulty of the quantum theory of radiation that any calculation of a process in a higher than the lowest possible order leads to divergencies.

[4] This case was first calculated with a correspondence method by C. Møller, Zeits. f. Physik **70**, 786 (1931) and Ann. d. Physik **14**, 531 (1932). The present method was first used for this problem by H. Bethe and E. Fermi, Zeits. f. Physik **77**, 296 (1932).

[5] P. Havas, Phys. Rev. **66**, 69 (1944). In the following referred to as I.

and

$$\mathbf{p}_1^0+\mathbf{p}_2^0+\cdots+\mathbf{p}_n^0+\mathbf{a}+\mathbf{b}+\cdots+\mathbf{z}+\mathbf{A}+\mathbf{B}+\cdots+\mathbf{Z}=\mathbf{p}_1^F+\mathbf{p}_2^F+\cdots+\mathbf{p}_n^F. \quad (6)$$

Here $E_n^0=(\mu^2+|\mathbf{p}_n^0|^2)^{\frac{1}{2}}$ and $E_n^F=(\mu^2+|\mathbf{p}_n^F|^2)^{\frac{1}{2}}$ denote the initial and final energy of the nth particle and $a\cdots z$ and $A\cdots Z$ are the energies of the light quanta with momenta $\mathbf{a}\cdots\mathbf{z}$ and $\mathbf{A}\cdots\mathbf{Z}$, respectively. We have written the equations in a form corresponding to absorptions only, but our calculations include emissions as well, as the only difference would be a change in sign throughout for the energy and momentum of the particular light quantum. Furthermore, we can include positrons as well as electrons by changing the sign of the energy and momentum of the particle.

The first non-vanishing matrix element for such a process is of the order $z+Z+2(n-1)$ in e. It involves $z+Z$ transitions caused by the interaction of the particles with all the light quanta and $n-1$ transitions due to the instantaneous Coulomb interactions of the particles. We obtain a matrix element of the same order if we have instead of the instantaneous Coulomb interaction of, say, the mth and the nth particle a retardation described by one transition corresponding to the emission of a light quantum K_{mn} by particle e_m and a second transition caused by the absorption of this quantum by e_n and *vice versa*.

Any succession of transitions involving the same light quantum more than once or more than $n-1$ Coulomb interactions would either be of a higher order than those just considered or would not fulfill the conditions (5) and (6). These conditions require furthermore that the $n-1$ Coulomb interactions are chosen in such a way that all n particles are involved, i.e., that we do not have one group of k particles, and another group of the remaining $n-k$ particles, interacting with the particles of their respective groups only. (This simply means that the number of *independent* equations for the momenta in the intermediate states has to equal the number of unknowns.)

We note that we cannot expect (3c) to give finite results for any values of the energies and momenta of the particles and quanta involved subject to the conditions (5) and (6) only. We assume for the moment that we have to deal with non-vanishing denominators of (3c) only and shall discuss the limitations of the first-order approximation later.

We do not attempt to sum over all possible successions of intermediate states since we want only to study the form of the retardation for a given Coulomb interaction. For this purpose it is sufficient to consider a typical portion of the sum consisting of all the terms belonging to a specific set of intermediate states of each particle, i.e., to sum over *all* the intermediate states of the *entire system* corresponding to *one* set of intermediate states of the *individual* particles. This is the part which has the same numerator in (3c), except the difference caused by instantaneous and retarded interaction. We have for the interaction of, say, e_m and e_n, apart from a common factor

$$2(u_m{}^{i*}u_m{}^{i+1})(u_n{}^{G*}u_n{}^{G+1})/|\Delta\mathbf{p}_{mn}|^2$$

for the instantaneous Coulomb interaction,

$$\sum_{\substack{\text{directions of}\\ \text{polarization}}}(u_m{}^{i*}\alpha K_{mn}u_m{}^{i+1})(u_n{}^{G*}\alpha K_{mn}u_n{}^{G+1})/K_{mn} \quad (7)$$

for the retardation,

with $K_{mn}=|\Delta\mathbf{p}_{mn}|$ the absolute value of the change in momentum of either particle caused by the Coulomb interaction, and similarly for the interaction of any other pair of particles.

We shall now consider our specific set of intermediate states in detail. In particular we shall focus our attention on one particle, e_m, say. To fix our ideas we assume that e_m first interacts with the light quantum a, then b, c, $\cdots i$. After the interaction with i, it interacts with another particle e_n whose preceding and following interactions were with the quanta G and H, say. Then e_m interacts with quantum j, k, $\cdots s$ and subsequently with a particle e_k whose preceding and following interactions were with the quanta R and S, say. Finally e_m interacts with t, u, $\cdots z$.

We denote the light quanta (and their energies) by small letters if they interact with the mth electron (in the part of the matrix element we are considering now) and by capital letters for all the other electrons. We shall not need to specify the other $n-3$ Coulomb interactions and the interactions of the other $n-1$ particles with the remaining $Z-4$ quanta; we shall only use the interactions of e_m as a guide to the structure of

our set of intermediate states and then derive the formulas for the summation in full generality.

We have already arbitrarily ordered the quanta which interact with e_m and also the quanta which interact with each one of the other particles (although we did not write down the order of interactions for each of the other particles explicitly). We still have to sum over all possible orders of interaction subject to these limitations, i.e., over all possible orders of interaction of the *different* particles. The only restriction beyond the arbitrary partial ordering of quanta mentioned above is that the Coulomb interaction of, say, e_m and e_n can only take place after e_m has interacted with the light quantum i and e_n with G, but before their interactions with j and H, respectively. The restriction for the case, that instead of the Coulomb interaction we have emission and absorption of K_{mn}, is that e_m can emit K_{mn} only after it has interacted with i and before interaction with j and that e_n can only absorb K_{mn} after interaction with G and before interaction with H (and *vice versa*). There is no further restriction on the choice of successions of intermediate states, and in particular the emission and absorption of K_{mn} need not take place in two consecutive steps.

Momenta and energies of the particles in the intermediate states are uniquely determined by (5) and (6), once we have arbitrarily chosen a set by fixing the order of interactions for each particle. Each intermediate state can be expressed as the sum of n states involving one particle only. These individual states however are not uniquely determined, as the problem imposes conditions for the summed expressions only and we are free to choose a set which is most convenient for our calculations.

We have seen that the denominator of (3c) contains the product of the energy differences of the initial (or final) and intermediate states. The corresponding differences of the momenta are zero. If we wish to split each intermediate state into a sum of n individual states we can impose the following condition to make this choice unique: *The momentum shall be conserved for each succession of individual intermediate states.*

We shall illustrate this by writing down the differences of energies and momenta for the individual intermediate states of e_m in our example. The initial momentum and energy are:

$$\mathbf{p}_1{}^0+\mathbf{a}+\mathbf{b}+\cdots+\mathbf{z} \text{ and } E_m{}^0+a+b+\cdots+z. \quad (8)$$

After absorption of a we have the following momentum and energy differences

$$\mathbf{p}_m{}^0-\mathbf{p}_m{}^a+\mathbf{a}(=0) \quad \text{and} \quad E_m{}^0-E_m{}^a+a,$$

where $E_m{}^a=(\mu^2+|\mathbf{p}_m{}^a|^2)^{\frac{1}{2}}$. We shall denote this energy difference by $\langle E_m{}^a\rangle$. Similarly we have after absorption of the quantum i

$$\mathbf{p}_m{}^0-\mathbf{p}_m{}^i+\mathbf{a}+\mathbf{b}+\cdots+\mathbf{i}(=0) \quad (9a)$$

and

$$E_m{}^0-E_m{}^i+a+b+\cdots+i=\langle E_m{}^i\rangle. \quad (9b)$$

Up to this point our self-imposed condition was fulfilled automatically as we were dealing with one particle only. Now however we have a Coulomb interaction with another particle e_n which changes $\mathbf{p}_m{}^i$ to $\mathbf{p}_m{}^{i+1}$. We denote $\mathbf{p}_m{}^{i+1}-\mathbf{p}_m{}^i$ $(=\mathbf{p}_n{}^G-\mathbf{p}_n{}^{G+1})$ by $\Delta\mathbf{p}_{mn}$ and instead of $\mathbf{p}_m{}^0-\mathbf{p}_m{}^{i+1}$ $+\mathbf{a}+\mathbf{b}+\ldots+\mathbf{i}$ which would not be equal to zero we write

$$\mathbf{p}_m{}^0-\mathbf{p}_m{}^{i+1}+\Delta\mathbf{p}_{mn}+\mathbf{a}+\mathbf{b}+\cdots+\mathbf{i}(=0). \quad (10a)$$

If we do not want to introduce an error in the summed expression, we have therefore to use $\mathbf{p}_n{}^0-\mathbf{p}_n{}^{G+1}-\Delta\mathbf{p}_{mn}$ instead of just $\mathbf{p}_n{}^0-\mathbf{p}_n{}^{G+1}$ in the set of individual intermediate states of particle e_n. Furthermore we have to use as our energy difference now in analogy to the expression for the momentum difference

$$E_m{}^0-E_m{}^{i+1}+\Delta E_{mn}+a+b+\cdots+i=\langle E_m{}^{i+1}\rangle^6 \quad (10b)$$

and similarly to subtract ΔE_{mn} in the corresponding expression for the particle e_n. But here we cannot take ΔE_{mn} as $E_m{}^{i+1}-E_m{}^i$ because then (10b) would be identical with (9b) and we would not have taken the Coulomb interaction into account at all. Furthermore this would destroy the symmetry in the treatment of the mth and nth particle, as $E_m{}^{i+1}-E_m{}^i$ is in general not equal to $E_n{}^G-E_n{}^{G+1}$. However we have not yet used the fact that $\Delta\mathbf{p}_{mn}$ can be expressed in terms of the *initial* and *final* momenta

[6] Up to $\langle E_m{}^i\rangle$ the notation is the same as in I. The expression corresponding to $\langle E_m{}^{i+1}\rangle$ however was denoted $\langle E_m{}^i\rangle$ there. We had to change the notation because now one particle can undergo more than one Coulomb interaction, and the former notation was not suitable for the general case.

of the particles and quanta as the momenta of all the particles in the intermediate states are uniquely determined by our choice of the order of the interactions for each particle. After we have formed this expression for $\Delta\mathbf{p}_{mn}$ we can now define a ΔE_{mn} analogously in terms of the initial and final energies. That is, if $\Delta\mathbf{p}_{mn}$ is a certain function of the initial and final *momenta* of the particles and quanta, then ΔE_{mn} is the *same* function of the initial and final *energies*. This resultant expression is in general not equal to $E_m^{i+1}-E_m^i$, as energy is not conserved for transitions to intermediate states.

We do not write down any explicit expressions for $\Delta\mathbf{p}_{mn}$ and ΔE_{mn} as they depend on our entire choice of orders of interactions. We note however, that for a given distribution of the interactions of the light quanta among the n particles and a fixed choice of the other $n-2$ Coulomb interactions $\Delta\mathbf{p}_{mn}$ and ΔE_{mn} for the interaction of e_m and e_n do *not* depend on the fact that this interaction takes place after interaction of e_m with i and of e_n with G. We shall need this fact in Section V.

Now we can again continue as before. After absorption of quantum s the momentum and energy differences will be given by

$$\mathbf{p}_m^0-\mathbf{p}_m^s+\Delta\mathbf{p}_{mn}+\mathbf{a}+\mathbf{b}+\cdots+\mathbf{s}(=0) \quad (11a)$$

and

$$E_m^0-E_m^s+\Delta E_{mn}+a+b+\cdots+s=\langle E_m^s\rangle. \quad (11b)$$

For the second Coulomb interaction we proceed as above and obtain

$$\mathbf{p}_m^0-\mathbf{p}_m^{s+1}+\Delta\mathbf{p}_{mn}+\Delta\mathbf{p}_{mk}+\mathbf{a}+\mathbf{b}+\cdots+\mathbf{s}(=0) \quad (12a)$$

and

$$E_m^0-E_m^{s+1}+\Delta E_{mn}+\Delta E_{mk}+a+b+\cdots+s=\langle E_m^{s+1}\rangle, \quad (12b)$$

where $\Delta\mathbf{p}_{mk}$ and ΔE_{mk} are defined analogously to $\Delta\mathbf{p}_{mn}$ and ΔE_{mn}.

Finally after absorption of the last quantum z we obtain

$$\mathbf{p}_m^0-\mathbf{p}_m^F+\Delta\mathbf{p}_{mn}+\Delta\mathbf{p}_{mk}+\mathbf{a}+\mathbf{b}+\cdots+\mathbf{z}(=0) \quad (13a)$$

and

$$E_m^0-E_m^z+\Delta E_{mn}+\Delta E_{mk}+a+b+\cdots+z=\langle E_m^F\rangle. \quad (13b)$$

By comparison of (13a) and (6) we obtain

$$\Delta\mathbf{p}_{mn}+\Delta\mathbf{p}_{mk}=\sum_{i\neq m}(\mathbf{p}_i^0-\mathbf{p}_i^F)+\mathbf{A}+\mathbf{B}+\cdots+\mathbf{Z}, \quad (14a)$$

and therefore

$$\Delta E_{mn}+\Delta E_{mk}=\sum_{i\neq m}(E_i^0-E_i^F)+A+B+\cdots+Z, \quad (14b)$$

which in combination with (5) shows that expression (13b) is equal to zero.[7]

Now our condition for determining the individual intermediate states appears less arbitrary. It has assured us first of all of a symmetrical treatment of all the particles and furthermore the initial and final states enter into the expressions symmetrically too. This latter symmetry for the *summed* expression is a consequence of the Hermitian character of the matrix element, but the summation will be somewhat easier to perform if we already define our individual intermediate states symmetrically.

We have now simplified our notation sufficiently to attempt the summation of our series for the case where we have only to deal with instantaneous Coulomb interactions. The case of retardation will be discussed after we have obtained the mathematical tools for the summation.

We might observe that if we had chosen an example where e_m interacts with more than two particles we would, after proceeding as above, have finally obtained two equations exactly analogous to (14a) and (14b), the only difference being that the left-hand sides would have consisted of the sums of more than two $\Delta\mathbf{p}$'s and ΔE's.

III. A THEOREM

Let

$$\begin{aligned} &Z_1^0=0;\ Z_1^1,\ \cdots Z_1^a;\ Z_1^F=0\\ &Z_2^0=0;\ Z_2^1,\ \cdots Z_2^b;\ Z_2^F=0\\ &\cdot\\ &\cdot\\ &\cdot\\ &Z_X^0=0;\ Z_X^1,\ \cdots Z_X^z;\ Z_X^F=0 \end{aligned}$$

be X sets of numbers Z_N^r.

[7] It should be noted that (13b) never appears in the denominator of (3c) by itself, so that its vanishing does not introduce any difficulty.

In addition to these X sets we are given $X-1$ pairs of elements $Z_L{}^{\lambda}$, $Z_R{}^{\rho}$ where $L \neq R$ and $\lambda, \rho \neq F$. We shall call these pairs *links* and say that the two sets, Z_L and Z_R, are *linked* between $Z_L{}^{\lambda}$, $Z_R{}^{\rho}$ and $Z_L{}^{\lambda+1}$, $Z_R{}^{\rho+1}$.

By a *transition* for an expression in the Z we mean either (1) the replacement of *one* $Z_N{}^{r}$ by $Z_N{}^{r+1}$, if $Z_N{}^{r}$ is not an element of a link, or (2) the replacement of the two elements $Z_L{}^{\lambda}$, $Z_R{}^{\rho}$ of a link by $Z_L{}^{\lambda+1}$, $Z_R{}^{\rho+1}$, respectively.

We now choose the $X-1$ links between the X sets such that they have no element in common and that the sets are not broken up into two or more groups of sets which are linked only with the sets of their respective groups.

Now we define $[Z_1, Z_2, \cdots Z_X]$ as any product of $a+b+\cdots+x$ factors of the form $Z_1{}^{a}+Z_2{}^{\beta}+\cdots+Z_X{}^{\xi}$ formed according to the following rule: We take as the first factor one which can be reached from

$$\sum_{N=1}^{X} Z_N{}^{0}(=0)$$

in one transition, and then obtain each subsequent factor by performing *one* other transition, the last factor being therefore one from which

$$\sum_{N=1}^{X} Z_N{}^{F}(=0)$$

can be reached in one transition.

If the numbers are such that none of the factors vanishes, we then have the following

Theorem: The sum of the reciprocals of all the possible $[Z_1, Z_2, \cdots Z_X]$ is

$$\mathbf{S}_{Z_1{}^{z}, \cdots Z_X{}^{z}} = \sum 1/[Z_1, Z_2, \cdots Z_X] = \frac{1}{Z_1{}^{1} \cdots Z_X{}^{z}}.$$

We shall prove the theorem by induction.

We first note that we have proved a special case of the theorem in I. If we take the two sets

$$A^0=0; \quad A^1, \cdots A^n; \quad A^F=0$$
$$B^0=0; \quad B^1, \cdots B^m; \quad B^F=0$$

with one link A^n, B^m, the series defined above is identical with the one defined in I (except for a slight change in notation). The sum of this series was there denoted by $S_{n,m}$ and proved to be equal to $1/A^1 \cdots A^n B^1 \cdots B^m$. Using this as a lemma, we can immediately prove that our theorem holds for any two sets of numbers with a link at an arbitrary position. We take two additional sets

$$A^0=0; \quad A^a, A^{a-1}, \cdots A^{n+1}; \quad A^F=0$$
$$B^0=0; \quad B^b, B^{b-1}, \cdots B^{m+1}; \quad B^F=0;$$

and if we now form our series for the combined sets

$$A^0=0; \quad A^1, A^2, \cdots A^n, A^{n+1}, \cdots A^a; \quad A^F=0$$
$$B^0=0; \quad B^1, B^2, \cdots B^m, B^{m+1}, \cdots B^b; \quad B^F=0$$

with a link between A^n, B^m and A^{n+1}, B^{m+1}, we obtain

$$\mathbf{S}_{A1, \cdots B^b} = S_{n,m} \cdot S_{n+1,m+1} = 1/A^1 \cdots A^a B^1 \cdots B^b.$$

We now assume the theorem to hold for X sets of numbers. Since there is necessarily at least one set with just one link, it is then sufficient to show that it remains true if we add another set of numbers

$$Z_Y{}^{0}=0; Z_Y{}^{1}, \cdots Z_Y{}^{y}; Z_Y{}^{F}=0$$

with just one link $Z_Y{}^{p}$, $Z_L{}^{q}$ say, of this new set with the other sets.

We now construct the new series. We collect those terms in which a factor containing $Z_Y{}^{p}$ appears before one containing $Z_L{}^{i+1}$ but after one containing $Z_L{}^{i}$, and also a factor containing $Z_Y{}^{p+2}$ before one containing $Z_L{}^{t+1}$ but after one containing $Z_L{}^{t}$. This part of our new series is the same as a series obtained according to the rules of our theorem from the original X sets except for replacing the set $Z_L{}^{0}=0; Z_L{}^{1}, \cdots Z_L{}^{l}; Z_L{}^{F}=0$ by the three sets

$$Z_{Y_1}{}^{0}=0; \quad Z_Y{}^{1}, \cdots Z_Y{}^{p-1}; \quad Z_{Y_1}{}^{F}=0$$

$$Z_L{}^{0}=0; \quad Z_L{}^{1}, \cdots Z_L{}^{i}, Z_L{}^{i}+Z_Y{}^{p}, Z_L{}^{i+1}+Z_Y{}^{p}, \cdots Z_L{}^{q}+Z_Y{}^{p}, Z_L{}^{q+1}+Z_Y{}^{p+1}, \cdots Z_L{}^{t}+Z_Y{}^{p+1}, Z_L{}^{t}, \cdots Z_L{}^{l}; \quad Z_L{}^{F}=0$$

$$Z_{Y_2}{}^{0}=0; \quad Z_Y{}^{p+2}, \cdots Z_Y{}^{y}; \quad Z_{Y_2}{}^{F}=0,$$

with links $Z_Y{}^{p-1}$, $Z_L{}^{i}$ and $Z_L{}^{t}+Z_Y{}^{p+1}$, $Z_{Y_2}{}^{0}$. If a link of the Z_L-set with another set contained $Z_L{}^{j}$ originally, it would now contain $Z_L{}^{j}+Z_Y{}^{p+1}$, if j is between i and $t-1$, and remain unchanged otherwise. If $p=0$ or $p+1=F$, we would have to omit the Y_1-set and one $Z_L{}^{i}$ or the Y_2-set and one $Z_L{}^{t}$, and our considerations would be independent of i or t, respectively.

Assuming the theorem still to hold after the addition of sets of less then p or $y-p-1$ non-

vanishing elements, we can sum and obtain

$$\frac{1}{Z_1{}^1\cdots Z_K{}^k Z_M{}^1\cdots Z_X{}^x Z_Y{}^1\cdots Z_Y{}^{p-1}Z_Y{}^{p+2}\cdots Z_Y{}^y}\times\frac{1}{Z_L{}^1\cdots Z_L{}^i(Z_L{}^i+Z_Y{}^p)\cdots(Z_L{}^q+Z_Y{}^p)(Z_L{}^{q+1}+Z_Y{}^{p+1})\cdots(Z_L{}^t+Z_Y{}^{p+1})Z_L{}^t\cdots Z_L{}^l}.$$

The second fraction is just the general term of a series formed from the two sets

$$Z_L{}^0=0;\quad Z_L{}^1,\cdots Z_L{}^i,\cdots Z_L{}^q, Z_L{}^{q+1},\cdots Z_L{}^t,\cdots Z_L{}^l;\quad Z_L{}^F=0,$$
$$Z_Y{}^0=0;\quad Z_Y{}^p, Z_Y{}^{p+1};\quad Z_Y{}^F=0,$$

with a link at $Z_L{}^q$, $Z_Y{}^p$. Letting i vary from 0 to q (except if $p=0$ as mentioned above) and t from $q+1$ to l (except if $p+1=F$) and summing, we obtain therefore for our series formed from Y sets

$$\mathbf{S}_{Z_1{}^1,\ldots Z_Y{}^y}=\frac{1}{Z_Y{}^1\cdots Z_Y{}^y}\mathbf{S}_{Z_1{}^1,\ldots Z_X{}^x}=\frac{1}{Z_1{}^1\cdots Z_Y{}^y}.$$

Now the addition of a set with no non-vanishing elements $Z_Y{}^0=0$, $Z_Y{}^F=0$ with one link $Z_Y{}^0$, $Z_L{}^q$, say, to a collection of X sets leaves the series of reciprocals unchanged and the theorem still holds for the new collection of sets. This completes the proof of our theorem.

IV. SUMMATION OF THE SERIES

We are now ready to perform the summations. Our $\langle E\rangle$'s as given by (9b), (10b), (11b), and (12b) and analogous expressions for the other individual intermediate states of e_m and similarly for the other $n-1$ particles are defined in such a way that our theorem can immediately be applied to the collection of sets of $\langle E_n\rangle$'s. We obtain, therefore, for the sum of the terms containing the instantaneous Coulomb interactions, omitting for the moment the factors common to the entire series

$$\frac{2^{n-1}(u_m{}^{i*}u_m{}^{i+1})(u_n{}^{G*}u_n{}^{G+1})(u_m{}^{s*}u_m{}^{s+1})(u_k{}^{R*}u_k{}^{R+1})\cdots}{|\Delta\mathbf{p}_{mn}|^2|\Delta\mathbf{p}_{mk}|^2\cdots}\times\frac{1}{\langle E_m{}^a\rangle\cdots\langle E_m{}^{s-1}\rangle\cdots}. \tag{15}$$

Now we shall discuss the changes introduced if the instantaneous interaction is replaced by the emission and absorption of a virtual quantum and we shall again investigate the intermediate states. The individual intermediate states are obviously not affected at all, as each particle still undergoes the same changes of momentum and energy as before. The only difference is that now the two particles do not change their momenta in a single transition. One particle suffers a change of momentum at the emission of the virtual quantum and the other at the absorption. Let us consider the transitions of e_m in our example in detail. Up to the absorption of quantum i everything is unchanged. Then the virtual quantum K_{mn} is emitted. This quantum is absorbed at some later stage by e_n. Our formalism allows a very simple description of this. We can introduce a new individual intermediate state for this virtual quantum; according to our convention about momenta our changes in momentum and energy then are given by

$$-\mathbf{K}_{mn}-\Delta\mathbf{p}_{mn}(=0), \tag{16a}$$
$$-K_{mn}-\Delta E_{mn}, \tag{16b}$$

and instead of our previous n sets of $\langle E\rangle$'s we have now the same sets plus a new set

$$0,\ -K_{mn}-\Delta E_{mn},\ 0.$$

Instead of the former link $\langle E_m{}^i\rangle$, $\langle E_n{}^G\rangle$ between the sets of $\langle E_m\rangle$'s and $\langle E_n\rangle$'s corresponding to the instantaneous interaction, we have two links with the new set corresponding to the emission and absorption of K_{mn}. The new set is linked with the $\langle E_m\rangle$'s between 0, $\langle E_m{}^i\rangle$ and $-K_{mn}-\Delta E_{mn}$, $\langle E_m{}^{i+1}\rangle$ and with the $\langle E_n\rangle$'s between $-K_{mn}-\Delta E_{mn}$, $\langle E_n{}^G\rangle$ and 0, $\langle E_n{}^{G+1}\rangle$; the sums of the reciprocals have still to be formed according to the rules of our theorem and we obtain again expression (15) except for an additional factor

$1/(-K_{mn}-\Delta E_{mn})$ and a change in the numerator (compare (7)).

We can proceed likewise for the case that K_{mn} is emitted by e_n and absorbed by e_m. This can be described by a new individual intermediate state with momentum and energy differences given by

$$+\mathbf{K}_{mn}+\Delta\mathbf{p}_{mn}(=0), \tag{17a}$$

$$-K_{mn}+\Delta E_{mn}, \tag{17b}$$

the momentum of the quantum being opposite to the one we had previously, the energy being the same. We have now an additional set

$$0,\ -K_{mn}+\Delta E_{mn},\ 0.$$

Instead of the former link between the $\langle E_m\rangle$'s and $\langle E_n\rangle$'s corresponding to the instantaneous Coulomb interaction, the $\langle E_n\rangle$'s are linked with the new set between $\langle E_n{}^G\rangle$, 0 and $\langle E_n{}^{G+1}\rangle$, $-K_{mn}+\Delta E_{mn}$, and similarly the $\langle E_m\rangle$'s between $\langle E_m{}^i\rangle$, $-K_{mn}+\Delta E_{mn}$ and $\langle E_m{}^{i+1}\rangle$, 0. We can sum as before, the only difference being the factor $1/(-K_{mn}+\Delta E_{mn})$ instead of $1/(-K_{mn}-\Delta E_{mn})$. Adding these two sums we obtain apart from a factor common with (15)

$$\frac{(u_m{}^{i*}\alpha K_{mn}u_m{}^{i+1})(u_n{}^{G*}\alpha K_{mn}u_n{}^{G+1})}{K_{mn}}\times\frac{2K_{mn}}{(\Delta E_{mn})^2-K_{mn}{}^2}. \tag{18}$$

Now we have to sum over the directions of polarization of K_{mn} and add the expressions for the instantaneous and the retarded interaction. As the independent directions of polarization are mutually perpendicular and perpendicular to the direction of propagation of K_{mn}, we have

$$\sum(u_m{}^{i*}\alpha K_{mn}u_m{}^{i+1})(u_n{}^{G*}\alpha K_{mn}u_n{}^{G+1}$$
$$=(u_m{}^{i*}\alpha u_m{}^{i+1})\cdot(u_n{}^{G*}\alpha u_n{}^{G+1})$$
$$-(u_m{}^{i*}\alpha\mathbf{K}_{mn}u_m{}^{i+1})(u_n{}^{G*}\alpha\mathbf{K}_{mn}u_n{}^{G+1})/\mathbf{K}_{mn}{}^2. \tag{19}$$

Remembering that $|\mathbf{K}_{mn}|=|\Delta\mathbf{p}_{mn}|$, we see finally from (15), (18), and (19) that by taking into account the retardation we simply have to replace the expression for the instantaneous interaction

$$\frac{4\pi\hbar^2c^2e_me_n}{|\Delta\mathbf{p}_{mn}|^2}(u_m{}^{i*}u_m{}^{i+1})(u_n{}^{G*}u_n{}^{G+1}), \tag{20}$$

by the expression

$$\frac{4\pi\hbar^2c^2e_me_n}{|\Delta\mathbf{p}_{mn}|^2-(\Delta E_{mn})^2}\Big\{(u_m{}^{i*}u_m{}^{i+1})(u_n{}^{G*}u_n{}^{G+1})-(u_m{}^{i*}\alpha u_m{}^{i+1})\cdot(u_n{}^{G*}\alpha u_n{}^{G+1})$$
$$+\frac{-(\Delta E_{mn})^2(u_m{}^{i*}u_m{}^{i+1})(u_n{}^{G*}u_n{}^{G+1})+(u_m{}^{i*}\alpha\Delta\mathbf{p}_{mn}u_m{}^{i+1})(u_n{}^{G*}\alpha\Delta\mathbf{p}_{mn}u_n{}^{G+1})}{|\Delta\mathbf{p}_{mn}|^2}\Big\}. \tag{21}$$

We have derived this expression by just considering the interaction between e_m and e_n. It can be seen immediately that the calculations for the next interaction (between e_m and e_k) would be completely analogous and that the calculations remain unchanged if we consider sums in which more than one instantaneous interaction is replaced by emission and absorption of a virtual quantum. We would simply have to add more than one set of states like (16) and (17), and we could apply our theorem with similar results to this more complicated collection of sets. Therefore, our result (21) is perfectly general. For that part of the matrix element we are considering the sum would then be an expression completely analogous to (15), but each factor of the form (20) being replaced by one of the form (21).

We can write (21) in another form which is more convenient for the further calculations. From the definition of $\Delta\mathbf{p}_{mn}$

$$\Delta\mathbf{p}_{mn}=\mathbf{p}_m{}^{i+1}-\mathbf{p}_m{}^i=\mathbf{p}_n{}^G-\mathbf{p}_n{}^{G+1}$$

and Dirac's equation

$$(\alpha\mathbf{p}_m{}^i+\beta\mu)u_m{}^i=E_m{}^iu_m{}^i,$$

for the ith state of the mth particle and similar equations for the other states and their complex conjugates we have[8]

$$u_m{}^{i*}\alpha(\mathbf{p}_m{}^{i+1}-\mathbf{p}_m{}^i)u_m{}^{i+1}=(E_m{}^{i+1}-E_m{}^i)u_m{}^{i*}u_m{}^{i+1}$$

and

$$u_n{}^{G*}\alpha(\mathbf{p}_n{}^G-\mathbf{p}_n{}^{G+1})u_n{}^{G+1}=(E_n{}^G-E_n{}^{G+1})u_n{}^{G*}u_n{}^{G+1},$$

[8] The analogous equation in I, p. 75 had some indices omitted erronously and should read

$$u_1{}^{0*}\alpha(\mathbf{p}_1{}^F-\mathbf{p}_1{}^0)u_1{}^F=(E_1{}^F-E_1{}^0)u_1{}^{0*}u_1{}^F=\Delta E\cdot u_1{}^{0*}u_1{}^F.$$

and therefore (21) becomes

$$\frac{4\pi\hbar^2c^2e_me_n}{|\Delta\mathbf{p}_{mn}|^2-(\Delta E_{mn})^2}\Big\{(u_m{}^{i*}u_m{}^{i+1})(u_n{}^{G*}u_n{}^{G+1})-(u_m{}^{i*}\alpha u_m{}^{i+1})\cdot(u_n{}^{G*}\alpha u_n{}^{G+1}) + \frac{[-(\Delta E_{mn})^2+(E_m{}^i-E_m{}^{i+1})(E_n{}^{G+1}-E_n{}^G)](u_m{}^{i*}u_m{}^{i+1})(u_n{}^{G*}u_n{}^{G+1})}{|\Delta\mathbf{p}_{mn}|^2}\Big\}. \quad (22)$$

V. REDUCTION TO MØLLER'S FORMULA

The first two terms of expressions (21) or (22) are identical with Møller's formula.[4] The last term however is not equal to zero except for the case of a process involving two particles only, which is just the one treated by Møller. If we wish to show that our result is identical with Møller's expression, we have to show that this last term cancels with terms from other parts of the matrix element. Therefore we must not limit ourselves to consideration of that part of the matrix element which corresponds to just one definite set of intermediate states for each individual particle. We can still however restrict ourselves to that part which involves the interaction of each particle with the same quanta and in the same order as before.

We shall continue to use our example. First we shall rewrite the numerator of the last term of (22). Using definitions (9b) and (10b) for the $\langle E_m\rangle$'s and the analogous definitions for the $\langle E_n\rangle$'s, we can write

$$-(\Delta E_{mn})^2+(E_m{}^i-E_m{}^{i+1})(E_n{}^{G+1}-E_n{}^G) = (\langle E_m{}^{i+1}\rangle-\langle E_m{}^i\rangle)(E_n{}^{G+1}-E_n{}^G) + \Delta E_{mn}(\langle E_n{}^{G+1}\rangle-\langle E_n{}^G\rangle). \quad (23)$$

We remember that the denominator of that part of the matrix element we were considering before contained the product

$$\cdots\langle E_m{}^i\rangle\langle E_m{}^{i+1}\rangle\langle E_n{}^G\rangle\langle E_n{}^{G+1}\rangle\cdots,$$

and we can see that (23) consists of four terms each having just one of these $\langle E\rangle$'s as a factor.

Let us consider the first of these terms in detail. We shall indicate all the factors containing the $(i+1)$th state of e_m and obtain

$$\frac{\langle E_m{}^{i+1}\rangle(E_n{}^{G+1}-E_n{}^G)(u_m{}^{i*}u_m{}^{i+1})(u_m{}^{i+1*}\alpha_j u_m{}^j)\cdots}{\cdots\langle E_m{}^{i+1}\rangle\cdots} \quad (24)$$

We can clear fractions and then sum over both signs of spin and energy of the $(i+1)$th state, using the well-known formula[9]

$$\sum_{p'}(u^*,0u^!)(u'^*,Qu'')=(u^*,0Qu'')$$

and obtain an expression which no longer contains any reference to this state.

Now let us consider a different part of the total matrix element, namely the one which contains exactly the same sets of intermediate states as the part previously considered, with one exception: Instead of the interaction between e_m and e_n taking place after e_m has interacted with the light quantum i and before interaction with j, this interaction shall take place after e_m has interacted with j, but not yet with k. Then, the only difference between the states of the new set and those of the old set will be that instead of the former $(i+1)$th state we have a new state of the mth particle, which we have to call the jth one to be consistent with the notation introduced previously, but which we shall distinguish from the previous jth state by placing it in a bracket [ ]. The new $[j+1]$th state will be identical with the old jth one, the new $[k]$th one with the old kth one, and so forth. If we now form the expression corresponding to (23), we obtain

$$(\langle E_m{}^{[j+1]}\rangle-\langle E_m{}^{[j]}\rangle)(E_n{}^{G+1}-E_n{}^G) + \Delta E_{mn}(\langle E_n{}^{G+1}\rangle-\langle E_n{}^G\rangle).$$

We now consider the second term of this expression, i.e., the one with $\langle E_m{}^{[j]}\rangle$ as a factor, and proceed as we did above with the first term. In place of (24) we have now

$$\frac{-\langle E_m{}^{[j]}\rangle(E_n{}^{G+1}-E_n{}^G)(u_m{}^{i*}\alpha_j u_m{}^{[j]})(u_m{}^{[j]*}u_m{}^{[j+1]})\cdots}{\cdots\langle E_m{}^{[j]}\rangle\cdots}. \quad (25)$$

[9] Compare, e.g., reference 1, p. 86, Eq. (25).

If we now sum over both signs of spin and energy of the $[j]$th state, we obtain an expression which just cancels with the one obtained from (24).

The generalization is obvious. By considering all the terms with the same set of intermediate states of e_n, but the interaction of e_m with e_n taking place after interaction of e_m with $a, b, \cdots s$ respectively, the terms of (23) containing the $\langle E_m\rangle$'s and the corresponding expressions cancel except for two terms which we have to treat separately. Similarly by considering all the terms with the same set of intermediate states of e_m, but the interaction of e_m with e_n taking place after interaction of e_n with $\cdots(G-1), G, H, \cdots$ the terms of (23) and the corresponding expressions containing the $\langle E_n\rangle$'s cancel.

The terms which have to be treated separately are the ones containing $\langle E_m{}^0\rangle$ and $\langle E_m{}^s\rangle$.

$\langle E_m{}^0\rangle$ is the factor of a term of the expression corresponding to (23) for the limiting case that the interaction between e_m and e_n takes place before e_m has interacted with any light quantum; there is no counterpart to this term, but remembering our definitions of the $\langle E_m\rangle$'s we see that $\langle E_m{}^0\rangle$ itself is zero and that $\langle E_m{}^0\rangle$ does not appear in the denominator, so that this term vanishes.

$\langle E_m{}^s\rangle$ is the factor of the first term of the expression corresponding to (23) for the other limiting case, namely that the interaction between e_m and e_n takes place after e_m has interacted with the first s light quanta (remembering that the interaction with $(s+1)$ takes place only after interaction of e_m with e_k). The expression analogous to (24) for this case is

$$\frac{\langle E_m{}^s\rangle(E_n{}^{G+1}-E_n{}^G)}{\cdots\langle E_m{}^s\rangle\cdots}(u_m{}^{s-1*}u_m{}^s)(u_n{}^{G*}u_n{}^{G+1})\Big\{(u_m{}^{s*}u_m{}^{s+1})(u_k{}^{R*}\cdot u_k{}^{R+1})-(u_m{}^{s*}\alpha u_m{}^{s+1})\cdot(u_k{}^{R*}\alpha u_k{}^{R+1})$$
$$+\frac{-(\Delta E_{mk})^2(u_m{}^{s*}u_m{}^{s+1})(u_k{}^{R*}u_k{}^{R+1})+(u_m{}^{s*}\alpha\Delta\mathbf{p}_{mk}u_m{}^{s+1})(u_k{}^{R*}\alpha\Delta\mathbf{p}_{mk}u_k{}^{R+1})}{|\Delta\mathbf{p}_{mk}|^2}\Big\}. \quad (26)$$

We can continue the above procedure by letting the interaction between e_m and e_k take place after interaction of e_m with $t, u, \ldots z$. All the terms will cancel as before, so that (26) is the only term remaining.

We then repeat the entire procedure with the only difference that we now let e_m interact with e_k before it interacts with e_n. We will again have cancellations as before; but we will have again one term left over from the case that e_m interacts with e_k after interaction with s, and then with $e_n, t, u, \cdots z$. This term will be

$$\frac{-\langle E_m{}^{[s]}\rangle(E_n{}^{G+1}-E_n{}^G)}{\cdots\langle E_m{}^{[s]}\rangle\cdots}(u_m{}^{[s]*}u_m{}^{s+1})(u_n{}^{G*}u_n{}^{G+1})\Big\{(u_m{}^{s-1*}u_m{}^{[s]})(u_k{}^{R*}u_k{}^{R+1})-(u_m{}^{s-1*}\alpha u_m{}^{[s]})(u_k{}^{R*}\alpha u_k{}^{R+1})$$
$$+\frac{-(\Delta E_{mk})^2(u_m{}^{s-1*}u_m{}^{[s]})(u_k{}^{R*}u_k{}^{R+1})+(u_m{}^{s-1*}\alpha\Delta\mathbf{p}_{mk}u_m{}^{[s]})(u_k{}^{R*}\alpha\Delta\mathbf{p}_{mk}u_k{}^{R+1})}{|\Delta\mathbf{p}_{mk}|^2}\Big\}, \quad (27)$$

and if we sum both (26) and (27) over both signs of spin and energy of the sth and $[s]$th state, respectively, we see that they cancel. This completes the proof that the first part of all the expressions (23) cancels and the proof for the second part is completely analogous. The generalization to the case of more than two Coulomb interactions of e_m is obvious; and in the case of just one Coulomb interaction, the difficulty connected with (26) would not have appeared at all.

Therefore we have proved that the *total* matrix element (3c) remains unchanged if we use instead of (21) or (22) simply the expression

$$\frac{4\pi\hbar^2c^2e_me_n}{|\Delta\mathbf{p}_{mn}|^2-(\Delta E_{mn})^2}\{(u_m{}^{i*}u_m{}^{i+1})(u_n{}^{G*}u_n{}^{G+1})$$
$$-(u_m{}^{i*}\alpha u_m{}^{i+1})\cdot(u_n{}^{G*}\alpha u_n{}^{G+1})\}, \quad (28)$$

as the matrix element for the retarded interaction of e_m and e_n in complete analogy with the matrix element for the instantaneous interaction (20). We recall that $|\Delta\mathbf{p}_{mn}|$ is the absolute value of the change in momentum of either particle and if we express this in terms of the initial and final

momenta of the particles and light quanta of the entire process (6), we obtain ΔE_{mn} from the corresponding initial and final energies from (5).

The part of the matrix element we considered in Section II becomes then in complete analogy to (15)

$$(-e)^{s+Z+2(n-1)}[(2\pi\hbar^2c^2)^{s+Z+2(n-1)}/(a\cdots zA\cdots Z)]^{\frac{1}{2}}\frac{\cdots(u_m{}^{0*}\alpha_a u_m{}^a)\cdots(u_m{}^{s-1*}\alpha_z u_m{}^F)\cdots}{\cdots\langle E_m{}^a\rangle\cdots\langle E_m{}^{s-1}\rangle\cdots}$$

$$\times\frac{2^{n-1}\cdots[(u_m{}^{i*}u_m{}^{i+1})(u_n{}^{G*}u_n{}^{G+1})-(u_m{}^{i*}\boldsymbol{\alpha}u_m{}^{i+1})\cdot(u_n{}^{G*}\boldsymbol{\alpha}u_n{}^{G+1})]\cdots}{\cdots[|\Delta\mathbf{p}_{mn}|^2-(\Delta E_{mn})^2]\cdots}. \quad (29)$$

To obtain the total matrix element we would have to consider all the different orders of interaction of the light quanta with each particle, all the different distributions of the light quanta among the different particles and for each of these cases all the different possibilities of having $n-1$ Coulomb interactions. Furthermore we would have to take the exclusion principle into account by making the total matrix element antisymmetric in the coordinates of the n particles. Finally we would have to sum over both signs of spin and energy of the electrons in the different intermediate states.

We are not concerned with this in this paper. We note however that the denominator of our final expression (29) contains only factors with just one particle in an intermediate state only in the denominator. Therefore the summation over both signs of the energy can be carried out by the method of Casimir,[10] which could not have been applied to the unsummed expression which contained factors with up to all n particles in intermediate states.

VI. DISCUSSION

Our expression (21) is identical with (4c), which was derived in I for the case of just two particles (but any number of light quanta) present, while we now have proved its validity in the presence of any number of particles and quanta. This expression has been obtained by summing over all intermediate states containing virtual quanta describing the retardation. While it could be used as a matrix element for the retarded interaction of two free particles, we have shown in Section V by carrying the summation one step further, that it is sufficient to use the simpler expression (28).

[10] H. Casimir, Helv. Phys. Acta **6**, 287 (1933).

Neither of these expressions is identical with the expression given in reference 1, p. 101, Eq. (31) and also in another paper,[11] except for the simplest possible case of just two particles and no radiation present.[4] This is due to the fact already pointed out in I, that the expression obtained by those authors is calculated by taking into account only those terms of the matrix element in which the quantum describing the retardation is absorbed in the transition immediately following the emission. It has been shown throughout this paper and also in I that this does not take into account all the possible successions of transitions of the same order in the electronic charge e. We shall however in the appendix discuss completely the process considered in reference 11 and write down the intermediate states for this case (collision of three particles) explicitly.

Expression (28) is identical with the expression obtained by Møller,[4] which until now had been thought to hold only in the case where two particles are present. In this simple case it is obtained by considering just one term in the matrix element corresponding to the emission of a virtual quantum by one and reabsorption by the other particle and another one with the role of the two particles interchanged. We have seen in the course of our calculations that for a more complicated process the retardation is described by a large number of terms, the exact number of which depends on the process under consideration, while we still can use the simple matrix element (4a) for the instantaneous interaction. This introduces an apparent difference in the treatment of instantaneous and retarded interaction and the analogy is restored only after

[11] W. Heitler and L. Nordheim, J. de phys. et rad. **5**, 449 (1934).

TABLE I. Intermediate states.

No.	Transitions		Difference of energy of initial (or final) and intermediate states		Partial sums
	a interacts with a_1	a_1 interacts with a_2	$E_1^0+E_2^0-E_1^1-E_2^F$		$\dfrac{4(u_1^{s*}u_1^1)(u_2^{s*}u_2^F)(u_1^{1*}u_1^F)(u_2^{s*}u_2^F)}{(E_1^0+E_2^0-E_1^1-E_2^F)\,\lvert\mathbf{p}^F-\mathbf{p}^0\rvert^2}$
I					
IIa	a interacts with a_1	a_1 emits K_{12}	$E_1^0+E_2^0-E_1^1-E_2^F$	$E_2^F-E_2^0-K_{12}$	
IIb	a interacts with a_2	a_2 emits K_{12}	$E_1^0+E_2^0-E_2^1-E_1^F$	$E_1^F-E_1^1-K_{12}$	$\dfrac{4(u_1^{s*}u_1^1)(u_2^{s*}u_2^F)(u_1^{1*}\alpha_{K_{12}}u_2^{1*})(u_2^{s*}\alpha_{K_{12}}u_1^F)}{(E_1^0+E_2^0-E_1^1-E_2^F)\,\lvert\mathbf{p}^F-\mathbf{p}^0\rvert^2\,[(E_1^F-E_2^0)^2-\lvert\mathbf{p}^F-\mathbf{p}^0\rvert^2]}$
IIc	a_1 emits K_{12}	a_1 interacts with a_2	$E_2^0-E_2^F-K_{12}$	$E_1^F-E_1^1-K_{12}$	
IIIa	a_1 emits K_{12}	a_1 interacts with a_2	$E_1^0-E_1^1-K_{12}$	$E_1^0+E_2^0-E_2^1-E_1^F$	
IIIb	a_2 emits K_{12}	a_2 absorbs K_{12}	$E_2^0-E_2^F-K_{12}$	$E_1^0+E_2^0-E_1^1-E_2^F$	$\dfrac{4(u_1^{s*}\alpha_{K_{12}}u_2^{1*})(u_2^{s*}\alpha_{K_{12}}u_1^F)(u_1^{1*}u_1^F)(u_2^{s*}u_2^F)}{(E_1^0+E_2^0-E_1^1-E_2^F)\,[(E_2^F-E_2^0)^2-\lvert\mathbf{p}^F-\mathbf{p}^0\rvert^2]\,\lvert\mathbf{p}^F-\mathbf{p}^0\rvert^2}$
IIIc	a_2 emits K_{12}	a_1 absorbs K_{12}	$E_1^0-E_1^1-K_{12}$	$E_2^F-E_2^0-K_{12}$	
IVa	a_1 emits K_{12}	a_2 absorbs K_{12} a_1 emits K_{12}	$E_1^0-E_1^1-K_{12}$ $E_2^0+E_2^0-E_1^1-E_2^F$	$E_2^F-E_2^0-K_{12}$	
IVb	a_1 emits K_{12}	a_2 absorbs K_{12} a_1 emits K_{12}	$E_1^0-E_1^1-K_{12}$ $E_1^0+E_2^0-E_1^1-E_2^F$	$E_1^F-E_1^1-K_{12}$	
IVc	a_2 emits K_{12}	a_1 absorbs K_{12} a_2 emits K_{12}	$E_2^0-E_2^F-K_{12}$ $E_1^0+E_2^0-E_2^1-E_1^F$	$E_2^F-E_2^0-K_{12}$	
IVd	a_2 emits K_{12}	a_1 absorbs K_{12} a_2 emits K_{12}	$E_2^0-E_2^F-K_{12}$ $E_1^0+E_2^0-E_2^1-E_1^F$	$E_1^F-E_1^1-K_{12}$	
Va	a_1 emits K_{12}	a_2 absorbs K_{12} a_1 emits K_{12}	$E_1^0-E_1^1-K_{12}$ $E_2^0-E_1^F-K_{12}-K_{12}$	$E_2^F-E_2^0-K_{12}$	
Vb	a_1 emits K_{12}	a_2 absorbs K_{12} a_1 emits K_{12}	$E_1^0-E_1^1-K_{12}$ $E_2^0-E_1^F-K_{12}-K_{12}$	$E_1^F-E_2^0-K_{12}$	
Vc	a_2 emits K_{12}	a_1 absorbs K_{12} a_2 emits K_{12}	$E_2^0-E_2^F-K_{12}$ $E_1^0+E_2^0-E_1^1-E_2^F-K_{12}-K_{12}$	$E_1^F-E_1^1-K_{12}$	
Vd	a_2 emits K_{12}	a_1 absorbs K_{12} a_2 emits K_{12}	$E_2^0-E_2^F-K_{12}$ $E_1^0+E_2^0-E_1^1-E_2^F-K_{12}-K_{12}$	$E_1^F-E_2^0-K_{12}$	
Ve	a_1 emits K_{12}	a_2 absorbs K_{12} a_1 emits K_{12}	$E_1^0-E_1^1-K_{12}$ $E_2^0-E_2^F-K_{12}-K_{12}$	$E_2^F-E_2^0-K_{12}$	
Vf	a_1 emits K_{12}	a_2 absorbs K_{12} a_1 emits K_{12}	$E_1^0-E_1^1-K_{12}$ $E_2^0+E_2^0-E_1^1-E_2^F-K_{12}-K_{12}$	$E_1^F-E_1^1-K_{12}$	
Vg	a_2 emits K_{12}	a_1 absorbs K_{12} a_2 emits K_{12}	$E_2^0-E_2^F-K_{12}$ $E_1^F-E_1^0-K_{12}-K_{12}$	$E_1^F-E_1^1-K_{12}$	
Vh	a_2 emits K_{12}	a_1 absorbs K_{12} a_2 emits K_{12}	$E_2^0-E_2^F-K_{12}$ $E_1^F-E_1^0-K_{12}-K_{12}$	$E_1^F-E_1^1-K_{12}$	

elimination of the virtual quanta (compare Eqs. (20) and (21)). This can be readily understood if we remember that the expression for the instantaneous Coulomb interaction in the Hamiltonian (2b) had been obtained also by a summation over the longitudinal waves.[12] However the elimination of the longitudinal waves was performed in the exact equations, and the matrix element (20) or (4a) obtained from the exact expression, while we had to reverse the procedure and eliminate the transverse virtual quanta in the matrix element (3c). The fact that a consistent treatment of this first-order approximation restores the analogy in the treatment of instantaneous and retarded interaction shows that at least this approximation has a reasonable behavior in spite of the hitherto unsolved difficulties connected with these equations. This is shown by another fact too, namely the relativistic invariance of (28). This result was not necessarily to be expected, since the relativistic invariance of the theory had been destroyed by omitting the divergent term $\sum_{i,k} e_i e_k / r_{ik}$ from the Hamiltonian (2a) arbitrarily (compare references 1 or 12). However by using only terms of the lowest order in e in the matrix element we have again excluded the well-known divergent 'self-energy' terms which correspond to emission and reabsorption of light quanta by the same particle. Our result shows that this second arbitrary subtraction has restored the relativistic invariance.

The possible divergencies due to the vanishing of one of the factors in the denominator of (29) are analogous to those discussed in I. They occur only for particular values of the energies and momenta and therefore do not introduce any fundamental difficulties.

We have (as customary) used the expression 'retarded interaction' throughout for lack of a better expression. In the two simple cases where the matrix element has been calculated with a

[12] E. Fermi, Rev. Mod. Phys. **4**, 131 (1932).

correspondence method,[4,13] it has been pointed out that the same results are obtained by using retarded potentials or any combination of retarded and advanced potentials (the sum of the coefficients being 1); furthermore the result includes spin-spin interactions for which no classical analogy exists.

The author wishes to thank Dr. J. G. Beckerley for his valuable criticism of the manuscript.

APPENDIX

We consider the collision of three particles. Conservation of momentum and energy requires

$$\mathbf{p}_1^0+\mathbf{p}_2^0+\mathbf{p}_3^0=\mathbf{p}_1^F+\mathbf{p}_2^F+\mathbf{p}_3^F \tag{30}$$

and

$$E_1^0+E_2^0+E_3^0=E_1^F+E_2^F+E_3^F. \tag{31}$$

We first consider that part of the matrix element which corresponds to the interaction of e_1 and e_2 and subsequent interaction of e_1 and e_3. There is only one intermediate state with energy

$$E_1^1+E_2^F+E_3^0 \tag{32}$$

with $E_1^1=(|\mathbf{p}_1^0+\mathbf{p}_2^0-\mathbf{p}_2^F|^2+\mu^2)^{\frac{1}{2}}$ and using (29) we obtain immediately

$$\frac{16\pi^2\hbar^4c^4e_1^2e_2e_3}{(E_1^0+E_2^0-E_1^1-E_2^F)[|\mathbf{p}_2^F-\mathbf{p}_2^0|^2-(E_2^F-E_2^0)^2][|\mathbf{p}_3^F-\mathbf{p}_3^0|^2-(E_3^F-E_3^0)^2]}$$
$$\times[(u_1^{0*}u_1^1)(u_2^{0*}u_2^F)-(u_1^{0*}\boldsymbol{\alpha}u_1^1)\cdot(u_2^{0*}\boldsymbol{\alpha}u_2^F)][(u_1^{1*}u_1^F)(u_3^{0*}u_3^F)-(u_1^{1*}\boldsymbol{\alpha}u_1^F)\cdot(u_3^{0*}\boldsymbol{\alpha}u_3^F)]. \tag{33}$$

The total matrix element is obtained by summing over all permutations of 1, 2, and 3. If the particles are equal, we still have to antisymmetrize.[14]

We shall now write down explicitly all the intermediate states needed if we do not use our summed expressions (28) and (29). These and the corresponding energy differences are summarized in Table I.

The last column of Table I contains the sums of those parts of the matrix element which have the same numerator (except for a common factor). Summing over the different directions of polarization and adding these four expressions we obtain

$$\frac{16\pi^2\hbar^4c^4e_1^2e_2e_3}{(E_1^0+E_2^0-E_1^1-E_2^F)[|\mathbf{p}_2^F-\mathbf{p}_2^0|^2-(E_2^F-E_2^0)^2][|\mathbf{p}_3^F-\mathbf{p}_3^0|^2-(E_3^F-E_3^0)^2]}$$
$$\times\{(u_1^{0*}u_1^1)(u_2^{0*}u_2^F)-(u_1^{0*}\boldsymbol{\alpha}u_1^1)\cdot(u_2^{0*}\boldsymbol{\alpha}u_2^F)+[-(E_2^F-E_2^0)^2(u_1^{0*}u_1^1)(u_2^{0*}u_2^F)$$
$$+(u_1^{0*}\boldsymbol{\alpha}(\mathbf{p}_1^0-\mathbf{p}_1^1)u_1^1)(u_2^{0*}\boldsymbol{\alpha}(\mathbf{p}_2^F-\mathbf{p}_2^0)u_2^F)]/|\mathbf{p}_2^F-\mathbf{p}_2^0|^2\}\{(u_1^{1*}u_1^F)(u_3^{0*}u_3^F)$$
$$-(u_1^{1*}\boldsymbol{\alpha}u_1^F)(u_3^{0*}\boldsymbol{\alpha}u_3^F)+[-(E_3^F-E_3^0)^2(u_1^{1*}u_1^F)(u_3^{0*}u_3^F)$$
$$+(u_1^{1*}\boldsymbol{\alpha}(\mathbf{p}_1^1-\mathbf{p}_1^F)u_1^F)(u_3^{0*}\boldsymbol{\alpha}(\mathbf{p}_3^F-\mathbf{p}_3^0)u_3^F)]/|\mathbf{p}_3^F-\mathbf{p}_3^0|^2\},$$

with $\mathbf{p}_1^1=\mathbf{p}_2^0-\mathbf{p}_2^F+\mathbf{p}_1^0$. If we now write down the term corresponding to interaction of e_1 and e_3 and subsequent interaction of e_1 and e_2, we obtain the same expression with 2 and 3 interchanged. Summing over both signs of E_1^1, it can be seen easily that all the terms cancel except those appearing in (33) and a term similar to (33) but with 2 and 3 interchanged.

We see that this relatively simple problem requires already 19 terms for the one obtained by using (29) and the calculation of any more complicated process would become extremely tedious. In reference 11, ten of the 19 terms were omitted (*IIc*, *IIIc*, *Va–h*) as only consecutive emissions and absorptions were taken into account.

[13] C. Møller, Proc. Roy. Soc. **152**, 481 (1935) (two particles and one light quantum).

[14] Compare, e.g., N. F. Mott and H. S. W. Massey, *The Theory of Atomic Collisions* (Oxford University Press; Oxford, 1933), Chapter XV.

Letters to the Editor

PROMPT publication of brief reports of important discoveries in physics may be secured by addressing them to this department. The closing date for this department is the third of the month. Because of the late closing date for the section no proof can be shown to authors. The Board of Editors does not hold itself responsible for the opinions expressed by the correspondents. Communications should not in general exceed 600 words in length.

The Ferromagnetism of Collective Electron Assemblies in a Metal with Overlapping Energy Bands

WILLIAM BAND
Yenching University, Peiping, China
October 4, 1945

STONER[1] has developed the theory of ferromagnetism of a collective electron assembly in a metal with a single conduction band, showing that spontaneous magnetization can occur if $k\theta^*/\zeta \geq \frac{2}{3}$, where $k\theta^*$ is the exchange energy of an electron with spin parallel to the direction of magnetization, and ζ is the Fermi limit in the conduction band.

In practice the ferromagnetics have two overlapping conduction bands, and it can be shown[2] that spontaneous magnetization can occur when $k\theta^*/\zeta_d \geq 4/3(1+b)$, where ζ_d is the energy gap in the almost-full d-band, and b is the ratio of the number of states in the d-band in excess of the number of electrons in the two conduction bands, to the sum of the number of vacancies in the d-band and the number of electrons in the s-band. Because in practice $\zeta_d \ll \zeta$ the new condition does not require so large an exchange energy term as the Stoner theory.

Ferromagnetics are, therefore, not simply those for which the spin exchange energy is specially large, but rather those for which the d-band is almost filled.

When temperature variation is included in the analysis, it is found that spontaneous magnetization can occur only if T is less than the Curie point T_c given by the universal curve:

$$y = 1.8(0.75-x)^{\frac{1}{2}} \cdot x,$$

where

$$y = (T_c/\theta^*)(1+b)^{-\frac{1}{2}}$$

and

$$x = (\zeta_{d0}/k\theta^*)/(1+b).$$

The Curie temperature thus vanishes at both ends of a definite range of ζ_{d0} values and has a maximum corresponding to the Co atom. Examination of the Curie points[3]

TABLE I. Values of $k\theta^*$ and the energy band ζ_{d0}.

Element	$k\theta^*$ ev	ζ_{d0} ev
Cu	0.22?	zero
Ni	0.217	0.04
Co	0.159	0.11
Fe	0.147	0.19
Mn	0.2?	0.25

of the ferromagnetic alloys of Cu, Ni, Co, Fe, Mn, and the Heusler alloys, now permits a fairly decisive estimate of $k\theta^*$ for these elements and also a rough picture of the d-band head forms.

In Table I, ζ_{d0} ev represents the equivalent depth of the vacant levels in the d-band, obtained by producing the curve with its actual height and gradient at the top of the occupied levels, down to zero with normal form proportional to the square root of the depth. Actual depths differ somewhat from equivalent depths because the form of the band-density curve is not normal.

The absence of ferromagnetism in such elements as Mn, Cu, Pd, Pt, and the alloys of Cu and Mn, is fully explained by the theory.

[1] E. C. Stoner, Proc. Roy. Soc. **A165** (1938); **A169** (1939).
[2] W. Band, "Collective Electron Assemblies in a Metal with Overlapping Energy Bands, Part I: General Theory."
[3] W. Band, "Collective Electron Assemblies in a Metal with Overlapping Energy Bands, Part II: The Occurrence of Ferromagnetism," both papers to appear in the Proceedings of the Cambridge Philosophical Society.

On the Theory of the Electron and of the Nucleon

A. PAIS
Institute for Theoretical Physics, University of Utrecht, Utrecht, Holland.
October 14, 1945

AS is well known, the classical Lorentz theory of the point electron is inconsistent inasfar as it gives rise to an infinite self-energy of the electron. This theory is unitary in the sense that the equation of motion of the electron is, for given initial conditions of the source functions, essentially a consequence of the electromagnetic field equations.

Grave self-energy difficulties are also inherent in quantum theory. For the following it is important to note that the quantum theory of the electron, like that of the nucleon, is non-unitary, though: the wave equation cannot be obtained from the quantized equations of the fields, produced by the particle concerned, as long as this particle is considered as a point the coordinates of which are taken as quantum variables.[1] As the wave equation which thus has to be introduced as an independent basic postulate into the theory involves the particle mass, the quantum self-energy W is a function of this quantity, contrary to classical (unitary) theory.

In an endeavor to overcome the divergence difficulties for electrons and nucleons within the framework of quantum field theory, I have follwed a method which consists in assuming these elementary particles to be the sources of sets of fields in such a way that the various infinite contributions to the self-energy, to which these fields give rise, cancel each other so as to make the final outcome finite. While this idea of mutual compensation appeared to be impracticable on a "one particle theory" (states of negative energy unoccupied), its application to hole theory to which the rest of this note exclusively refers, leads to the following results.

A. ELECTRONS

It has been examined whether W can be made finite by assuming the electron to be the source of a neutral short

range field (range κ^{-1}) besides the electromagnetic field. As the implicit equation for m: $W=mc^2$ would lead to $\kappa^{-1}\sim 10^{-68}$ cm, a quite unfamiliar value, while, moreover, it will turn out below that this relation would lead to inconsistencies with respect to further applications of the theory, we consider W as a perturbation compared with mc^2. The circumstance that the electron mass thus is essentially "mechanical" must be considered as a fundamental implication of the non-unitarity of the theory.

For all Kemmer types of fields (charged or neutral) one can introduce an interaction depending only on the meson field wave functions ("f-interaction") and one depending only on the first derivatives of these functions ("g-interaction"). By generalizing an argument due to Weisskopf[2] it can be shown that, in a development with respect to (charge)$^2/\hbar c$, f-interactions lead to logarithmic (log) divergences only, to any order of approximation. g-interactions yield in first approximation a quadratic (qu) and a log divergence.[3]

The introduction of a "subtractive" short range vector field with f-interaction, similar to Bopp's classical endeavor,[4] appears to yield a finite W (to any order of approximation) if the "convergence relation" $e^2=f^2$ is satisfied (e=electric charge, f=charge of the electron due to its coupling with the short range field). It can be shown that this convergence relation, like all other convergence relations mentioned in this note, is relativistically invariant. However, subtractive fields are incompatible with a stable vacuum distribution of electrons as required by hole theory. Thus they have to be discarded within the present interpretation of hole theory.

The further investigation of convergence relations has been confined to the first approximation, the question whether they also hold in higher approximations is still an open one. For a scalar f-coupling it has been found that

$$e^2=\tfrac{1}{4}f^2, \tag{1}$$

and that $W\ll mc^2$ if κ^{-1} is roughly $\approx r_0$, the classical electron radius.

b. NUCLEONS

In the wave equation of nucleons we put the mass term equal to βMc^2, i.e., we do not *a priori* distinguish between the proton mass M_P and the neutron mass M_N. The term $\Delta=M_P-M_N$ appears *a posteriori* in the theory as a self-energy term.

For an arbitrary set of meson fields responsible for nuclear interaction, the convergence relations are for the

$$\text{proton}\begin{cases}e^2+L=0\\ Q=0\end{cases}\qquad \text{neutron}\begin{cases}L=0\\ Q=0\end{cases} \tag{2}$$

The L-(Q-)relations are necessary to eliminate the log (qu) divergences. Clearly the L-relations for proton and neutron are incompatible. Compatibility is obtained, however, if the proton, like the electron, also is assumed to create a scalar "f-field"—in accordance with the requirement of f-charge conservation applied to $N\rightarrow P+e^-+n$, etc. For then (2) becomes $e^2-\tfrac{1}{4}f^2+L=0$ or $L=0$, in virtue of (1).

Δ can now (at any rate in first approximation) be computed as the sum of electromagnetic and f-self-energy of the proton. One finds $\Delta=-1.25m$ if $\kappa^{-1}=r_0$, or $\Delta=-1.90m$ if $\kappa^{-1}=3r_0$: Δ has the right sign and order of magnitude if a reasonable value of κ is adopted. It should be stressed that the assumption $W=mc^2$ for the electron leads to grave inconsistencies with respect to Δ.

The discussion of $L=0$, $Q=0$ reveals that none of the most habitual meson theories of nuclear forces yields finite self-energies. As examples of theories which do lead to finite W (at any rate in first approximation) we mention: Hulthén's pseudoscalar-scalar theory[5] and the set of fields proposed by Møller and Rosenfeld, again combined with a scalar field. In both cases this scalar field (which from the point of view of convergence plays a similar role as the f-field but should not be confused with it) is neutral and its range considerably shorter than that of the other meson fields. It is tempting to identify this field with the neutral interaction of very short range that, according to Hulthén,[6] should be introduced to interpret the angular distribution of high speed neutrons by protons.

It appears that the nucleon self-energies are always $\ll Mc^2$. Thus *all quantum field self-energies are perturbations compared to the corresponding mechanical masses.*

Finally two consequences of the f-field hypothesis may be mentioned: according to (1) the Coulomb potential of the hydrogen atom is modified to

$$-\frac{e^2}{r}(1-2e^{-\kappa r}),$$

yielding a hydrogen S-level shift of

$$\Delta\nu(nS)\approx\frac{8\alpha^6}{n^3}\cdot\frac{1}{\kappa^2 r_0^2}\cdot\frac{mc}{\hbar}\ \text{cm}^{-1},\quad \alpha=\frac{1}{137}.$$

The shift for $n=2$ reported by Williams-Pasternack[7] is obtained for $\kappa^{-1}=2.5\,r_0$. Further the f-quanta are unobservable as their life-time in the rest system is (cf. (1))

$$\frac{1}{2\alpha\kappa c}\sim 10^{-21}\ \text{sec}.$$

Full details will be given in a paper, "On the Theory of Elementary Particles," the publication of which has been delayed considerably by war circumstances and which will appear as soon as practicable.

[1] Pryce, Proc. Roy. Soc. **A159**, 355 (1937).
[2] V. F. Weisskopf, Phys. Rev. **56**, 72 (1939).
[3] The calculations of W by Kemmer, Proc. Roy. Soc. **A166**, 127 (1938), have appeared to be incorrect.
[4] Bopp, Ann. d. Physik **38**, 345 (1940); **42**, 575 (1943); cf. also A. Landé and L. H. Thomas, Phys. Rev. **60**, 121, 514 (1940).
[5] Hulthén, Fysiogr. Sellsk. Lund **14**, 2 (1944).
[6] Hulthén, Arkiv Mat. Astr. og Fys. **29a**, no. 33 (1943).
[7] Williams, Phys. Rev. **54**, 558 (1938); Pasternack, ibid. **54**, 1113 (1938).

Width of Resonance Process in Boron (11)

JAMES F. MARVIN
Departments of Physics and Biophysics, University of Minnesota, Minneapolis, Minnesota
October 10, 1945

AN attempt was made to determine the true width of the resonance process of the long range alpha-particles from the first of the alternate reactions

$$B^{11}+H^1\rightarrow Be^8+He^4,$$
$$\rightarrow 3\,He^4.$$

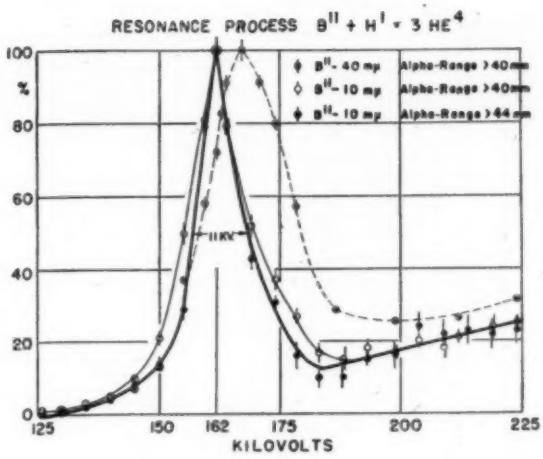

FIG. 1.

The present data are offered in corroboration of the data of Kanne, Taschek, and Ragan[1] on the position of the resonance peak, and of Jacobs and Whitson[2] on the shape of the yield curve. Data on the width of the resonance are offered, in which constancy of the voltage is not a factor. (Figure 1.)

The resistance controlled transformer-kenotron condenser set[3] was used to supply voltage up to 225 kilovolts. Ripple of approximately 4.5 kilovolts[4] was reduced to about 100 volts by loading the set with five condensers of capacity 0.5 mf each, tapped onto the potential divider. Voltage was monitored manually with a deviation of less than ±1 kilovolt. Voltage was measured with a high resistance voltmeter, calibrated in sections with the aid of a potentiometer and standard cell to an accuracy of 0.5 percent.

Targets were of boron (11), on a polished copper button, prepared by Hoff Lu[5] with a high intensity mass spectrograph. One target had boron deposited to a thickness of 10 millimicron (mμ) and another a thickness of 40 mμ. Heating of the targets, as recommended by Bowersox,[6] prevented deposition of carbon on the 10 mμ target. The 40 mμ target had some abuse before the present experiment, but no further deposition occurred after it was heated. Thus, the yield curves remained constant during the course of the experiment.

Alpha-particles were observed at 90°, with the targets at a 45° angle. A shallow ionization chamber was used. Observations were made at ranges of 40 and 44 millimeters to make certain the long range alpha-particles appearing at energies of over 180 kilovolts could not be accounted for by the slight increase in range of the continuous group of alpha-particles from the second alternate reaction due to the greater kinetic energy of the bombarding protons. That the two curves for 40 and 44 millimeters range agree settles this point. Slight deviations are noted, however, in the region of 175 kilovolts.

The yield curves indicate, as shown by Jacobs and Whitson, a sharp resonance superimposed on an exponentially increasing background. The theoretical aspects of this phase of the problem have been discussed by Wheeler.[7]

The proton energy required at the resonance peak is 162±1 kilovolts. This value agrees with that of Kanne, *et al.* (163±6 kilovolts). Other values given have varied from 159 to 165 kilovolts. Higher values than these have been shown to be in error because of deposition of carbon on the targets.

The experimental half-width at half-maximum of the resonance for the 10-mμ target is 5.5 kilovolts. This width cannot be a broadening of the resonance due to variation in the voltage. Ripple was 100 volts, and variation in voltage for other reasons was held to ±1 kilovolt. Half-width for the 40-mμ target is 10.5 kilovolts. This agrees with the value of 1.6 kilovolts for the stopping power of the 10-mμ target. The third factor in the experimental broadening of the resonance is the presence of scratches in the polished copper button. Heidenreich and Matheson[8] have utilized the electron microscope for the study of polished steel surfaces. They have demonstrated the presence of scratches of depth 13–50 mμ. The presence of such scratches would give an apparent thickness to the target which would readily account for the observed width of the resonance. It seems reasonable to conclude, therefore, that the width of the resonance is considerably less than the minimum measured width.

[1] W. R. Kanne, R. F. Taschek, and G. L. Ragan, Phys. Rev. **58**, 693 (1940).
[2] J. A. Jacobs and W. L. Whitson, Phys. Rev. **A59**, 108 (1941).
[3] J. H. Williams, W. H. Wells, J. T. Tate, and E. L. Hill, Phys. Rev. **51**, 434 (1937).
[4] J. S. Allen, R. O. Haxby, and J. H. Williams, Phys. Rev. **A53**, 325 (1938).
[5] Hoff Lu, unpublished.
[6] R. B. Bowersox, Phys. Rev. **55**, 323 (1939).
[7] J. A. Wheeler, Phys. Rev. **59**, 27 (1941).
[8] R. D. Heidenreich and L. A. Matheson, J. App. Phys. **15**, 423 (1944).

Electron Beams in Strong Magnetic Fields

J. R. PIERCE
Bell Telephone Laboratories, New York, New York
October 12, 1945

IN a recent paper,[1] Brillouin derives some types of electron flow in beams and states several conclusions. It should be emphasized that these conclusions do not apply to beams derived from a cathode of finite size located in the magnetic field unless the cathode is everywhere parallel to the magnetic field.

Consider, for instance, a circular disk cathode and axially symmetrical accelerating electrodes, the whole system immersed in a strong uniform magnetic field perpendicular to the cathode. Assuming no component of electric field in the θ direction we have from the angular momentum equation

$$\dot{\theta}=\frac{\omega_0}{2}(1-(r_0/r)^2). \tag{1}$$

Here $\omega_0=(e/m)B$ and r_0 is the radius at which the electron leaves the cathode. We have also

$$\ddot{r}-r\dot{\theta}^2=-(e/m)E_r-\omega_0^2\dot{\theta}. \tag{2}$$

Here E_r is the radial field, which may be due to space charge or to the accelerating voltages applied to the electrodes.

Letting $r-r_0=y$, $|y|\ll r_0$ (later to be justified by the result), we obtain the approximate equation

$$\ddot{y}=-(e/m)E_r-\omega_0^2 y. \tag{3}$$

As this is linear, the solution for $\dot{y}=y=0$ at $t=0$ is

$$y=-\frac{e}{m\omega_0}\int_0^t E_r(T)\sin\omega_0(t-T)dT. \tag{4}$$

Here $E_r(T)$ is the radial field the electron encounters a time T after it has left the cathode.

Equation (4) can be integrated by parts. Using the information that E_r is zero at the time $T=0$ when the electron leaves the cathode surface, we obtain

$$y=-\frac{e}{m\omega_0^2}\left\{E_r(t)-\int_0^t\cos\omega_0(t-T)d[E_r(T)]\right\}. \tag{5}$$

Now when $\omega_0=0$ (contrary to our assumption) the integral has the value $E_r(t)$. If $E_r(T)$ is a smoothly increasing function of T, as ω_0 is made larger and larger the integral will become smaller and smaller. For very large values of ω_0 the electron motion will be essentially a displacement outward (as E_r is negative).

$$y=-\frac{e}{m\omega_0^2}E_r(t), \tag{6}$$

and a rotation of angular velocity

$$\dot{\theta}=-\frac{e}{m\omega_0 r_0}E_r(t). \tag{7}$$

Thus the effect of making the magnetic field very intense is to make the electron paths approach straight lines normal to the cathode.

It is interesting to note that the electron optical equations for paraxial rays without space charge can be extended by means similar to those described by Meyer[2] and Condon[3] to give results similar to those of Brillouin but for focused beams in which the radius may change along the beam. Such a treatment would predict the final behavior of the beam in terms of the conditions under which it is generated.

[1] Leon Brillouin, "A Theorem of Larmor and its Importance for Electrons in Magnetic Fields," Phys. Rev. 67, 260–266 (1945).
[2] L. M. Meyer, *Electron Optics* (D. Van Nostrand Company, Inc., New York, 1939), p. 117.
[3] Edward U. Condon, "Focusing of Space Charge Limited Electron Beams," talk in A.I.E.E. Electron Ballistics Symposium, Columbia University, May 23, 1945.

Ionization by Fission Fragments in Nitrogen, Argon, and Xenon

N. O. Lassen
Universitetets Institut for Teoretisk Fysik, Copenhagen, Denmark
September 15, 1945

SEVERAL investigators using ionization chambers have determined the energy of fission fragments[1,2] by comparing the ionization produced by the fragments with that produced by α-particles and assuming proportionality between energy and ionization. This proportionality is known to be valid for α-particles, but as the fission fragments have much higher energies, masses, and charges than α-particles and as it is known,[3,4] that the mechanism of ionization is somewhat different for the two sorts of particles the assumption might seem to be a little problematic. Meanwhile, the results agree fairly well with other measurements of the energy,[5] as well as with the theory,[6] and thus we may consider the assumption to be correct, at least within some 10 percent. Nevertheless, it may be of interest to note that by measuring the ionization in different gases we get almost the same energy distribution of the fission fragments, which further confirms the correctness of the assumption.

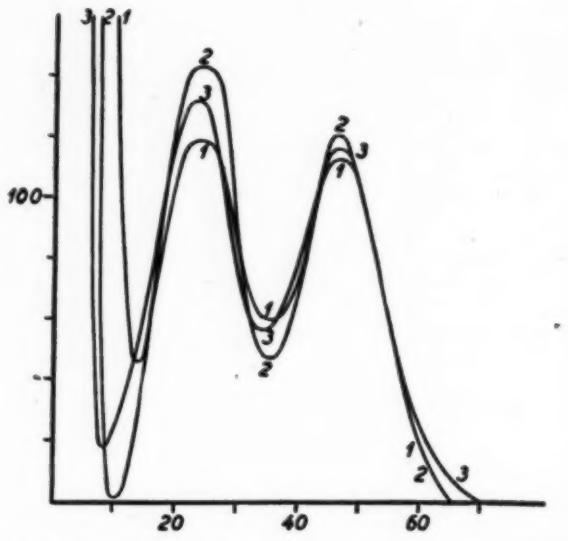

FIG. 1. Energy distribution of fission fragments having traversed 0.79 mg/cm² of mica+0.25 mg/cm² of aluminum. Measurements in nitrogen (curve 1), argon (curve 2), and xenon (curve 3).
Abscissa: Energy of Fragments in Mev
Ordinate Number of Fragments Per Unit Energy Range

Using the apparatus previously described[7] the ionization of fission fragments having traversed 0.79 mg/cm² of mica +0.25 mg/cm² of aluminum was determined. In Fig. 1, curve 2, the number of fragments is plotted against the size of the ionization pulses. The curve refers to 2,000 particles and is obtained with argon in the ionization chamber; in the previous letter[7] a second measurement was shown and there the experimentally found points were plotted. With nitrogen in the chamber we get a similar curve, but the pulses are much lower; this curve is transformed into curve 1 on the figure by multiplying the abscissae by 1/0.69 and the ordinates (in order to get the same area) by 0.69. In the same way curve 3 is obtained from the curve measured in xenon by multiplying the abscissae with 1/1.21 and the ordinates with 1.21. The figures 0.69 and 1.21 are chosen so as to make the end parts of the curves coincide; then, as seen, the curves almost coincide in the whole region occupied by fission fragments. The large number of small pulses represents the background in the ionization chamber produced by neutrons and especially by γ-rays.

The abscissae of the two peaks corresponding to the two groups of fission fragments and the valley between them are for all three curves very nearly the same and the

TABLE I.

Ratio of ionization in the gases:	Earlier measurements α-particles Schmieder	Naidu	Gurney	This work α-particles	Fission fragments
N_2:A	0.675	0.67	0.71	0.68	0.69
Xe:A		0.97	1.22	1.18	1.21

differences may be ascribed to uncertainty due to statistical errors; also, the differences in the ordinates are only slightly larger than could be explained by uncertainty, but it is remarkable that curve 2 (argon) has the highest maxima and the lowest minimum, while the opposite is valid for curve 1 (nitrogen). This indicates that the straggling is lowest in argon and highest in nitrogen.

By use of the same ionization chamber the ratio between the ionization produced by α-particles from ThC and ThC′ in nitrogen and argon was found to be 0.68±0.03. In order to minimize the consumption of xenon a second ionization chamber of smaller volume was used to compare the ionization in xenon and argon by α-particles; the ratio was found to be 1.18±0.05. These figures are in good agreement with earlier results for α-particles given by Schmieder,[8] and by Gurney,[9] while the agreement with the work of Naidu[10] is not perfect. The figures are given in Table I.

The measurements were carried out at the Institute of Theoretical Physics in Copenhagen and I wish to express my best thanks to the Director of the Institute, Professor Niels Bohr, as well as to Professor I. C. Jacobsen for placing the cyclotron at my disposal and for the excellent working conditions. My thanks are also due to Mr. Søren Madsen and to Mr. Alex. Holst, Director of Norsk Hydro, who presented the argon and the xenon.

[1] M. H. Kanner and H. H. Barchall, Phys. Rev. **57**, 372 (1940).
[2] Flammersfeld, Gentner, and Jensen, Zeits. f. Physik **120**, 450 (1943).
[3] N. Bohr, Phys. Rev. **59**, 270 (1941).
[4a] Bøggild, Brostrøm, and Lauritzen, Kgl. Danske Vid. Sels. Math-Fys. Medd. **18**, 4 (1940).
[4b] Bøggild, Brostrøm, and Lauritzen, Phys. Rev. **59**, 275 (1941).
[5] M. C. Henderson, Phys. Rev. **56**, 703 (1939).
[6] N. Bohr and J. A. Wheeler, Phys. Rev. **56**, 426 (1939).
[7] N. O. Lassen, a previous Letter to the Editor, Phys. Rev. **68**, 142 (1945).
[8] Schmieder, Ann. d. Physik **35**, 445 (1939).
[9] Gurney, Proc. Roy. Soc. **107**, 337 (1925).
[10] Naidu, J. de phys. et rad. **5**, 575 (1934).

Effect of Ultraviolet Light on Glass Containing Silver

A. E. BADGER AND F. A. HUMMEL
Department of Ceramic Engineering, University of Illinois, Urbana, Illinois
September 29, 1945

IT was pointed out several years ago by H. E. Ives that the Lippmann color photograph process could be used to produce plates which would reflect monochromatic light when illuminated with white light. Additional investigations of this phenomenon were conducted by R. W. Wood.

In some of our work dealing with colorless silicate glasses containing small amounts of silver, we have found that ultraviolet light will cause the silver to precipitate in the glass if the latter is maintained at a temperature of about 400°C. The colloidal silver produces an amber colored glass. Without illumination with ultraviolet light, the temperature necessary to cause the color to "strike" is considerably higher.

We have made some attempts to produce standing waves in colorless glasses containing silver by forming a platinum mirror on one face of a polished disk which was then heated in a furnace to about 400°C. Light from a quartz-mercury arc lamp was used to illuminate the disk through the open top of the furnace. If silver were precipitated at the antinodes of the standing waves, we might expect that the treated glass would reflect the mercury spectrum. However, no such result could be observed. This failure is ascribed to the low concentration of silver (*ca.* ¼ percent) in the glass.

Another interesting speculation is the possibility of producing a glass surface which would not reflect visible light by illumination with filtered ultraviolet light under the above conditions.

Ultrasonic Dispersion and Absorption in Hydrogen

ELLEN SWOMLEY STEWART, JAMES L. STEWART, AND J. C. HUBBARD
Johns Hopkins University, Baltimore, Maryland
November 6, 1945

MEASUREMENTS made in this laboratory with the variable-path ultrasonic interferometer show that there is a region of dispersion of the velocity of sound in hydrogen at ordinary temperatures and pressures beginning in the frequency region of 4–6 Mc. Illustrative values are given in Table I.

TABLE I. Velocity of sound in H_2 at 25°C.

f(Mc)	p(Atmos.)	V(m/sec.)	±S.D. of mean, (percent)
3.855	1.00	1321.9	0.082
	.50	1349.9	0.31
6.254	1.00	1365.0	0.24
	.50	1382.0	0.26
Classical		1315.8	

The increase in velocity is accompanied by an increase in absorption which is 10–25 times the already large classical value. This anomalous absorption has already been observed by van Itterbeek[1] and co-workers at lower frequencies and temperatures, but was not accompanied by reproducible observation of dispersion of velocity.

These effects are attributed to lag of energy exchange to and from the rotational states of the hydrogen molecule. Application of the theory, for example, Kneser's[2] dispersion formula, to these results, gives an inflection point in the V^2 *vs.* $\log f$ curve at 10.95±8 percent Mc and places the upper limit of the dispersion region at about 40 Mc.

Complete reports will be submitted soon.

[1] A. van Itterbeek and P. Mariens, Physica **4**, 609 (1937); A. van Itterbeek and L. Thys, Physica **5**, 889 (1938); A. van Itterbeek and R. Vermaelen, Physica **5**, 345 (1942).
[2] H. O. Kneser, Ann. d. Phys. [5] **11**, 777 (1931).

On the Decay Process of Positive and Negative Mesons

M. CONVERSI, E. PANCINI, AND O. PICCIONI
Instituto di Fisica della R. Università di Roma Centro di Fisica nucleare del C.N.R., Rome, Italy
October 15, 1945

SOME years ago Tomonaga and Araki[1] pointed out that on account of the electrostatic interaction with nuclei, the capture probability should be for negative mesons in dense material much greater than the decay probability; while for positive mesons the decay probability should prevail on the capture probability.

In 1941 in a direct measurement of the mean-life of mesons stopped in Al-absorber, Rasetti[2] obtained for the ratio η between decay-processes and stopped mesons the value $\eta=0.42\pm0.15$. Successively Auger, Maze, and Chaminade[3] found no essential lack from unity for η. Further experiments by Rossi and Nereson[4] (Al absorber), and by ourselves[5] (Fe absorber) gave, respectively, $\eta=0.4$ and $\eta=0.49\pm0.07$.

From the above mentioned works it seems reasonable to conclude that η is about 0.5. However, some doubt can be raised against the precision of such a value of η, considering that it is deduced from the comparison between its evaluated value and the rate of the actually registered decay-electrons, which represent only a small fraction of all the decay-processes occurring in the absorber.

Among other sources of error affecting the evaluation of η, one ought to consider the determination of the minimum delay of the registered electrons which depends on the size and shape of the counter-pulses. In order to avoid such a difficulty, in our previous work[5] we counted the delayed coincidences with little and slightly different delays and obtained from the plotted results the point "zero" of the time-scale. In order to obtain an independent determination of η and to check at the same time whether, according to Tomanaga and Araki prediction, negative mesons do not undergo the decay-process in dense materials, we performed an experiment based on the possibility of concentrating positive and negative mesons by means of magnetized iron cores.

The registering set—whose circuit has been already described in a previous paper[6]—consisted of three-fold (III) delayed-coincidences and of an anticoincidences unit. (This unit was really a four-fold (IV) coincidences unit.) It registered the decay-electrons, due to mesons stopped in a Fe absorber 3 cm thick. By means of convenient magnetized iron cores we could concentrate on this absorber alternatively positive or negative mesons. The energy of such mesons was well defined as that corresponding to the range interval between 20 cm of iron (magnetized iron cores) and 20+3 cm (absorber). We took care that the value of the magnetic induction B inside the magnetized iron cores was high enough ($B\approx15{,}000$ gauss) to concentrate on or bend away from the absorber all mesons of such an energy.

With a fixed delay we found the following results:

Concentrating positive mesons:

$$(\text{III–IV})_+=58/177^{h}\,16'=0.33\pm0.04,$$

Concentrating negative mesons:

$$(\text{III–IV})_-=13/168^{h}\,06'=0.077\pm0.02.$$

Regarding the actual result only as a qualitative one, we have not taken into account the small lack of efficiency of the four-fold coincidences.

These results point out the greatly different behavior of negative and positive mesons, so that the prediction of Tomonaga and Araki seems to be confirmed experimentally. We have not yet checked whether the small rate $(\text{III–IV})_-$ is caused by some instrumental effect, or not. Further experiments are now in progress.

[1] S. Tomonaga and G. Araki, Phys. Rev. **58**, 90 (1940).
[2] F. Rasetti, Phys. Rev. **60**, 198 (1941).
[3] Auger, Maze, and Chaminade, Comptes rendus **213**, 381 (1941).
[4] B. Rossi and N. Nereson, Phys. Rev. **62**, 417 (1942).
[5] M. Conversi and O. Piccioni, Nuovo Cimento II, 71 (1944); Phys. Rev. (submitted for publication).
[6] M. Conversi and O. Piccioni, Nuovo Cimento II, 40 (1944).

On a Type of Kinematical "Red-Shift"

E. L. HILL
University of Minnesota, Minneapolis, Minnesota
September 29, 1945

THE work of Page and Milne on the introduction of accelerated coordinate systems in relativity theory has recently been put on a more definite basis by the explicit reduction of the transformations involved to the 4-dimensional conformal group.[1] One of the important points thus introduced is the necessary use of a 15-parameter group of transformations, whereas the corresponding classical group requires but thirteen. The purpose of this note is to indicate an interpretation of one of these new parameters which leads to a type of "red-shift" phenomenon. We use the notation of reference 1 and leave aside transformations based on X_{15}, since these do not lead directly to velocity changes. If we consider an observer situated at the origin of coordinates, but having neither velocity nor acceleration, we can still modify his coordinate system by the 1-parameter subgroup of transformations based on X_{14}. To first orders this yields the equations

$$\mathbf{r}'=(1-\alpha_{14}t)\mathbf{r},\quad t'=t-\alpha_{14}\cdot\tfrac{1}{2}(t^2+r^2/c^2),$$

which, in turn, lead to the velocity formula

$$\begin{aligned}\mathbf{v}'&=\mathbf{v}-\alpha_{14}[\mathbf{r}-\mathbf{v}(\mathbf{r}\cdot\mathbf{v})/c^2]\\&=\mathbf{v}-\alpha_{14}\mathbf{r},\text{ to terms in }v^2/c^2.\end{aligned}$$

To this order of approximation the added term is a simple radial velocity with magnitude proportional to the distance from the observer. The sign of the velocity may be either positive or negative, and to obtain formal agreement with the observed red-shift we take $\alpha_{14}=-1.8\times10^{-17}$ sec.$^{-1}$. At very great distances, at which the radial velocity approaches that of light, the term in v^2/c^2 acts to limit the speed, but its effect is too small to be observable at present, since it amounts to only about 0.01 km/sec. at a distance of 2×10^{6} parsec., at which the red-shift gives a radial speed of around 1000 km/sec. In any event the first-order approximation which has been used here would become invalid, and the calculation would need to be carried out more exactly.

The Doppler shift of the light emitted from a distant point may be attributed in a conventional manner to the alteration in the emission time of a signal with the coordinate system, since

$$\Delta t' = (1-\alpha_{14}t)\Delta t,$$

where $t=r/c$ is now the travel time of the signal from the source to the observer.

The structure of the conformal group shows that this type of transformation is introduced as soon as one expands the Lorentz group by adjoining to it the transformations to accelerated axes, owing to the non-commutativity of the velocity and acceleration transformations. This procedure in turn rests on the hypothesis that the invariance of the Maxwell field equations is a fundamental physical requirement.

While a more complete analysis of the physical interpretation of the full group of transformations will be required before all of its implications can be appreciated, the simple treatment given here does seem to strengthen Milne's idea of an approach to the red-shift phenomenon without an explicit appeal to the relativistic theory of gravitation.

[1] E. L. Hill, Phys. Rev. 67, 360 (1945).

The Pair Production of Light Mesons by Electrons

H. FESHBACH AND L. TISZA
Physics Department, Massachusetts Institute of Technology, Cambridge, Massachusetts
October 19, 1945

IN a recent series of seminars given at the Massachusetts Institute of Technology, M. Schein discussed certain experiments in cosmic rays which seemed to indicate the existence of mesons of low mass of about 20 electron masses. The development of the betatron has made available a source of electrons of sufficiently great energy to make the laboratory production of these mesons feasible.

The mesons may originate either in the meson field or in the electric field associated with a nucleus. In this note we shall compute the second effect only, inasmuch as the only unknown constant involved is the meson mass whereas the first effect would also involve the unknown interaction between nucleons and light mesons. The method of virtual quanta, as given for example by E. J. Williams,[1] is used. In this procedure an electron of energy E may be replaced by a photon field such that the number of photons with an energy between ϵ and $\epsilon+d\epsilon$ is:

$$N(\epsilon)d\epsilon=\frac{2\alpha}{\pi}\left(\ln\frac{E}{\epsilon}\right)\frac{d\epsilon}{\epsilon}, \qquad (1)$$

$$\alpha=e^2/\hbar c.$$

These photons will under the influence of the Coulomb field of a nucleus produce meson pairs. The cross section for this process for "scalar" particles[2] of spin 0 and for particles[3] of spin $\hbar/2$ is

$$Q(\epsilon)=Z^2\alpha\left(\frac{e^2}{\mu c^2}\right)^2\left[A\ln\frac{2\epsilon}{\mu c^2}-B\right], \qquad (2)$$

where Z is the charge of the nucleus, μ = meson mass, $A=16/9$, $B=104/27$ for spin 0, and $A=28/9$, $B=218/27$ for spin $\hbar/2$. The cross section for the total process, the pair production of mesons by electrons becomes:

$$\sigma=\int^E N(\epsilon)Q(\epsilon)d\epsilon\sim\frac{A}{3\pi}(\alpha Z)^2\left(\frac{e^2}{\mu c^2}\right)^2\left(\ln\frac{E}{\mu c^2}\right)^3. \qquad (3)$$

A similar formula has been derived[4] for the case of the production of an electron-positron pair by an electron. It differs from (3) with $A=28/9$ only in the replacement of the meson mass by the electron mass. Formula (3) is valid only when both the energy of the incident electrons and the emitted mesons is high compared to their rest mass. Moreover the energy lost by the electron should be small compared to its initial energy.

When the incident electron energy is 100 Mev, the meson mass is 20 electron masses, and the nucleus $Pb(Z=82)$ then for scalar mesons, $\sigma\sim2\times10^{-28}$ cm^2 while for spin $\hbar/2$ mesons $\sigma\sim3\times10^{-28}$ cm^2.

It should be emphasized that formula (3) underestimates the total cross section since only one of the possible processes in which mesons can be produced is calculated. In addition, if the mesons were of the vector type, i.e., of spin $\hbar$, one would judge by analogy with the known meson bremstrahlung formulae[5] that the cross section for the pair production of vector mesons is greater than that given by (3).

[1] E. J. Williams, Kgl. Danske Vid. Sels. Math.-Fys. Medd. 13, 4 (1935).
[2] W. Pauli and V. Weisskopf, Helv. Phys. Acta. 7, 709 (1934).
[3] W. Heitler, *Quantum Theory of Radiation* (Oxford University Press, Oxford, 1936), p. 200.
[4] See reference 3, p. 203.
[5] R. F. Christy and S. Kusaka, Phys. Rev. 59, 405 (1941).

Method of Increasing Betatron Energy

DONALD W. KERST
Physics Department, University of Illinois, Urbana, Illinois
November 15, 1945

CONVENTIONAL betatrons used to date have followed the conservative designs similar to those described previously.[1,2] In these betatrons the flux density at the orbit of the electron is limited to a value less than half of the flux density which can be used in the center of the orbit. These betatrons have customarily been operated with approximately 4000 gauss at the orbit and 11,000 or 12,000 gauss in the iron within the orbit. This distribution of flux was necessary to have an equilibrium orbit at radius, r, since the flux, ϕ, within the orbit must satisfy $\phi-\phi_0=2\pi r^2H$. ϕ_0 is the flux linking the orbit when the field at the orbit is zero. With the conventional machine, ϕ_0 is zero.

The purpose of this letter is to point out that the flux, ϕ_0, need not be zero when the electrons are injected; it can be biased reversely so that the flux through the center of the orbit has a large negative value initially and changes to a large positive value during the acceleration process. Thus, since the maximum flux density in the center of the orbit can be made to change by twice the conventional amount, the field at the orbit and hence the final energy

of the electrons can be twice as great with a biasing flux. Geometrical factors due to the introduction of biasing coils for the biasing system will not allow a full factor of 2 to be achieved in a machine of a given pole diameter.

The biasing can most easily be achieved when used in conjunction with a closed central gap in the betatron. To close the magnet gap in the center of the orbit a back-wound coil about this center piece of iron but within the orbit is necessary. This can be connected in series with the main coils, and it must so reduce the ampere turns about the low reluctance central piece of iron that the flux condition $\phi - \phi_0 = 2\pi r^2 H$ is not exceeded. If the back-winding contains fewer turns than the total on the main coils, then a slight air gap left in the center may be used to adjust the flux condition.

This back-winding can reduce the energy which must be stored in the magnetic field and in the condensers to one-third of that in a non-back-wound betatron. The low reluctance of the central flux path requires few ampere turns of direct current for flux biasing. The biasing current may flow through the central back-wound coil, through both back-wound and all or part of the main coils, or through a separate coil around the poles. A choke coil generally is needed in the direct current circuit to block an alternating current except in case the right fraction of the main coil is in series with the back-wound coil to cancel the a.c. voltage.

A serious inadequacy of these methods, if applied to a betatron having a minimum of focusing region and a maximum closed gap area for the central flux, is that the orbit will vary in radius during acceleration as a result of non-linearity of the magnetic characteristics of iron. Much experience has shown the variation to be serious, and decreasing or eliminating the central air gap will make the variation worse; thus steps must be taken to make the flux condition hold. This can be accomplished by connecting in parallel two coils, one about the central flux and one about the complete pole having fewer turns than the coil about the central flux. The turn ratio must be chosen so that if the proper flux condition holds, then the voltage across the two coils is the same and hence they could be connected in parallel. Any deviation from the proper flux distribution then causes a circulating current which tends to restore the proper flux condition. The error in the flux forcing system is a result of the resistive voltage drop in the coils. This error is proportional to $\int_0^t IR dt$. Thus the resistance of the coils and the current through the coils must be held to a minimum. It is calculated that this method of flux forcing will hold the variation in radius to approximately one percent for the design we are interested in using.

Early in 1942 considerations for back-winding and flux biasing a betatron of approximately 250 Mev were begun. While the details of constructing such a betatron were being worked out this summer, information from Germany indicated that a similar plan was being drawn up there for a 200 Mev betatron, including back-winding, biasing, and the use of magnetic focusing lenses along the orbit. Apparently no flux forcing was contemplated.

[1] D. W. Kerst, Phys. Rev. **60**, 47–53 (July 1, 1941).
[2] D. W. Kerst, Rev. Sci. Inst. **13**, 387–394 (Sept., 1942).

Proceedings of the American Physical Society

Meeting of the New England Section at Springfield, Massachusetts, October 13, 1945

THE twenty-fifth meeting of the New England Section of the American Physical Society was held at the Springfield Division of Northeastern University in Springfield, Massachusetts, on Saturday, October 13, 1945. At least sixty members were in attendance. The program included five short papers and three invited papers. There follow the titles of the invited papers and the abstracts of those short papers which dealt with research problems, while those dealing with problems of teaching physics will appear in the *American Journal of Physics*.

At the business meeting the following officers were elected for 1946:

Chairman, S. R. Williams, *Amherst College.*
Vice Chairman, Henry Margenau.
Secretary-Treasurer, Gordon Ferrie Hull, Jr.
Programme Committee, Noel Little, V. E. Eaton, Robley D. Evans.*

Mildred Allen
Secretary-Treasurer

Invited Papers

Experiments with U H F Wave Guides. Gordon Ferrie Hull, Jr., *Dartmouth College.*

Jet Propulsion and Gas Turbines for Aircraft. A. F. Yacovone, *Pratt and Whitney Aircraft Division of United Aircraft Corporation.*

Radar—Principles and Applications That Can Now Be Told. W. B. Nottingham, *Massachusetts Institute of Technology.*

Contributed Papers

Radiochemical Changes in Some Fatty Acids. Richard E. Honig, *Massachusetts Institute of Technology.*—The effects of terrestrial radioactivity on the genesis of petroleum have been studied during the past three years under American Petroleum Institute Project 43c. Likely source materials investigated include a number of long chain fatty acids which were bombarded with alpha-particles from radon and with deuterons from the M.I.T. cyclotron. While the bombardment residue has been partially identified as a paraffin hydrocarbon only for the case of palmitic acid, $C_{15}H_{31}COOH$, and lauric acid, $C_{11}H_{23}COOH$,[1] analyses of the gaseous products from all acids investigated were readily carried out on a small Nier-type 60° mass spectrometer and were checked by a low temperature condensation and absorption method. In every case, the main constituents were H_2, CO_2, CO, and H_2O vapor, while CH_4, C_2H_6, C_3H_8, and C_4H_{10} were present only in very small amounts. These results show clearly that the radiochemical decomposition of a long chain fatty acid molecule occurs preferably by C—C bond rupture at the terminal COOH group. The absence of large amounts of gaseous paraffins indicates that the other C—C bonds are very rarely broken. The production of H_2 is much smaller than might be expected from consideration of the large number and relative strength of C—H bonds. It is interesting to note that the abundance of H_2 relative to CO_2 and CO increases linearly with the number of C—H bonds available in the molecule.

[1] C. W. Sheppard and W. L. Whitehead, Bull. Am. Assoc. Pet. Geol. (in press, 1945).

Analysis of Gas Mixtures with the Mass Spectrometer. Earle C. Farmer, *Massachusetts Institute of Technology.* (*Read by title.*)—Initially, the mass spectrometer was used primarily for measuring the abundance of isotopes. Recently this instrument has become a valuable analytical tool in determining the components of gas mixtures.[1] Under American Petroleum Institute Project 43c, the gaseous products from radiochemical studies of organic compounds have been analyzed with a Nier-type, 60° spectrometer developed for this purpose by Dr. R. E. Honig. Mixtures of water vapor, hydrogen, carbon dioxide, carbon monoxide, and saturated hydrocarbons up to and including the C_4 group have been studied. The mass spectra consist of a number of intensity peaks which result from the numerous molecular fragments formed in the ionizing region of the spectrometer. Neon is used as an internal, absolute standard of intensity. The pattern of these peaks is characteristic of the molecular structure of the gases in the mixture. Calibration with pure gases is necessary. The mass spectrum of an unknown mixture is interpreted in terms of the mass spectra of its several components. By the judicious selection of peaks which represent a single component, length calculations involving the solution of multiple simultaneous equations are avoided.

[1] H. W. Washburn, H. F. Wiley, and S. M. Rock, Ind. Eng. Chem. 15 (1943).

* At the business meeting, also, a vote of thanks was tendered to Dr. Allen for her able guidance of, and service to, the New England Section as Secretary-Treasurer during the most difficult years of its history.—K. K. D.

Large Currents through the Glass Envelope of an Incandescent Lamp Due to Electron Emission from the Filament. G. F. HULL, SR., *Hanover, New Hampshire.*— Probably all physicists while reading about the "Edison Effect" have wished that they could insert a metal plate inside an ordinary incandescent lamp and thus observe the electron emission. Probably several physicists have tried to draw the electrons through the glass envelope but have not obtained an appreciable current due to faulty technique or to the fact that the bulb used had a thick wall. K. S. Lion[1] recently reported obtaining initial currents of 2×10^{-7} ampere dropping to 6×10^{-8} and then rising to a maximum of 4×10^{-6} ampere. The writer has obtained currents nearly 100 times these amounts and has observed changes in the glass which are worth noting. Strips of metal foil are laid over the "polar cap" of a lamp bulb covering almost all the surface above the "equator." At first tin foil was used. It was satisfactory for a 50-watt lamp but was vaporized by the heat of a 75- or 100-watt lamp. Silver leaf (2.2×10^{-5} cm thick) is not vaporized and is more satisfactory. Strips of aluminum 1 mil thick are laid over the foil or silver leaf and a thin copper strip, closely fitting round the equator, holds all the strips in place and makes contact with most of the area above the equator. This copper strip is connected to the positive terminal of the 220-volt filament with a multirange sensitive ammeter in circuit. Before the current is turned on the filament, but with 220 volts in the "plate" circuit, a leakage current of about 2×10^{-6} amp. is noted. This is 20 times the initial current Lion found for emission. In all cases this leakage current should be measured. For an alternating voltage on the filament terminals, as in Lion's case, the d.c. leakage would be zero. As the positive terminal is 220 volts above the negative, the *average* voltage drawing the electrons to the plate is 110 volts but the three half power law enters to increase this voltage. An extra or boosting voltage may be inserted, but the voltage between the negative terminal of the filament and the polar cap or "plate" must be measured by a vacuum tube or electronic voltmeter. Lamps used were 50-watt frosted bulbs, and 75- and 100-watt both frosted and clear glass. The 50-watt gave the largest current. After 5 minutes average voltage 110, the current is steady at about 0.3 milliampere. Covering the plate with glass wool or asbestos ran the current up to 0.6 milliampere. For an average voltage of 330 these became 0.6 milliampere and 2 milliamperes. Fanning the plate lowers the current. For the 75- and 100-watt lamps, both frosted and clear glass, the currents obtained were about half of those for the 50-watt lamps. Yet the temperatures of the glass were decidedly higher—high enough to vaporize tin foil, which did not occur with the 50-watt lamps. The 75- and 100-watt clear glass bulbs did not change in appearance but the 50-watt frosted bulbs (no clear glass ones were used at 50 watts) were greatly changed after an hour's use. The upper part of the bulb was darkened, the lower part seemed to be covered with a dark steel gray deposit, and the emission current decreased with time. The experiment demonstrates the large currents that may be obtained through the glass due to emission from the filament, and it shows the great change in conductivity of the glass due to temperature change.

[1] K. S. Lion, Am. J. Phys. 11, 297 (1943).